Journal of Ocean Engineering and Marine Energy (2020) 6:303–337
https://doi.org/10.1007/s40722-020-00175-7

REVIEW ARTICLE

Boundary element and integral methods in potential flow theory: a review with a focus on wave energy applications

Louis Papillon[1] · Ronan Costello[2] · John V. Ringwood[3]

Received: 2 April 2020 / Accepted: 14 September 2020 / Published online: 27 September 2020

Abstract
This paper presents a comprehensive review of boundary element methods for hydrodynamic modelling of wave energy systems. To design and optimise a wave energy converter (WEC), it is estimated that several million hours of WEC operation must be simulated. Linear boundary element methods are sufficiently fast to provide this volume of simulation and high speed of execution is one of the reasons why linear boundary element methods continue to underpin many, if not most, applied wave energy development efforts; however, the fidelity of the physics included is inadequate for some of the required design calculations. Judicious use of non-linear boundary element methods provides a route to increase the fidelity of the modeling while maintaining speed and other advantages over more computationally demanding alternatives such as Reynolds averaged Navier–Stokes (RANS) or smooth particle hydrodynamics (SPH). The paper presents some background to each aspect of the boundary methods reviewed, building up a relatively complete theoretical framework. Both linear and nonlinear methods are covered, and consideration is given to the computational complexity of the methods reviewed. The paper aims to provide a review that is useful in selection of the most appropriate techniques for the next generation of WEC design tools.

Keywords Wave energy converter design tools · Potential flow theory · Boundary element method · Zero forward speed problem · Wave energy converter

1 Introduction

Despite continuous attention from both commercial and academic researchers over the past 50 years, wave energy has still not achieved large-scale commercialisation. It is evident that the development of economically attractive WEC technology is a difficult endeavour. Analysis of the reasons why wave energy research is so difficult and why it remains inconclusive at this time has been reported in detail by Weber (2012) and Weber et al. (2013). A new R&D management approach, more suited to the challenges of wave energy development, has been followed from Weber (2012) and Weber et al. (2013) and is further developed in Bull et al. (2016), Roberts et al. (2017), Weber and Laird (2018) and Costello et al. (2019). This new R&D management methodology may be termed the performance before readiness approach, since it emphasises the importance of achieving high-technology performance level (TPL) at low-technology readiness level (TRL) to increase overall performance and to reduce risks due to premature large-scale testing of new technologies. This performance before readiness methodology relies implicitly on heavy use of simulation and optimisation to provide low-cost evaluation of multiple instances of multiple candidate technologies while at low TRL.

Previous work, related to the present paper, has explored a wider set of CFD techniques that might be used in the next generation of wave energy design tools (Davidson and Costello 2020). That review targeted CFD techniques with the fidelity of included physics (and also computation time), intermediate to linearized potential flow (LPF), and RANS. The present paper presents a narrower but more detailed review of a particularly relevant subset of these CFD techniques, closer to LPF than to RANS, but still encompassing non-linear methods, namely Boundary Element and Integral Methods in Potential Flow.

✉ John V. Ringwood
john.ringwood@mu.ie

Louis Papillon
louis.papillon67@gmail.com

1 Ecole Centrale Nantes, Nantes, France

2 Wave Venture, Cork, Ireland

3 Centre for Ocean Energy Research, Maynooth University, Maynooth, Ireland

1.1 Place of simulation in wave energy R&D

Central to the performance before readiness approach to wave energy R&D is the visualisation of research progress as a trajectory on the TRL–TPL plane (see Fig. 1 and a further important concept is the partitioning of the TRL–TPL plane into a low-TRL left-hand domain and a high-TRL right-hand domain (Weber 2012). In the low-TRL left-hand side, R&D activities are relatively low cost and low risk, the performance before readiness approach holds that technology fundamentals should flexible and the imperative is innovation with an emphasis on evaluation and optimisation of many alternative designs. Conversely, in the high-TRL, right-hand domain, R&D activities are high cost and high risk, technology fundamentals should be fixed and the imperative in these activities is risk management rather than innovation. The usages of simulation tools differ in these left and right domains of the TRL–TPL plane. In the left-hand, low-TRL domain, the use of simulation is for evaluation and optimisation of many alternative designs while in the right-hand, high-TRL domain, the use of simulation is primarily concerned with risk mitigation, in particular quantification of environmental loading and adequacy of structural dimensioning in a singular prototype design rather than many alternative candidates. In this paper, we are primarily focused on methods suitable for the former use case but, nevertheless, the methods reviewed may also be suitable for the latter.

The combination of stochastic wave inputs and large number of design decision variables means that the number of simulations required to characterise the performance of a technology in a certain location is large. On the right-hand of Fig. 1 representing the high-risk, high-TRL, domain, this will often be in the thousands of runs while in the left-hand, low-risk, low-TRL domain, this can run into the millions of runs. This level of simulated time precludes the use of hi-fidelity RANS or SPH type simulation and motivates the use of more computationally efficient approaches. This need for computational efficiency explains the widespread use of phenomenological models based primarily on LPF in wave energy research. These models have served the wave energy sector well but have drawbacks related to the invalidation of underlying assumptions in the presence of large body motions (accentuated by control systems as in (Giorgi et al. 2016)) and in high and steep waves. In addition, present implementations of these methods suffer from non-physical results at so-called "irregular frequencies" (or"irregular values"), corresponding to the eigenfrequencies of the interior homogeneous Dirichlet problem (Ohmatsu 1975).

Given the emphasis placed on low-TRL assessment and optimisation in the performance before readiness approach, it follows that a key requirement for WEC simulation tools is suitability for use in the calculation of objective functions in automatic optimisation. To satisfy this requirement, Davidson and Costello (2020) state that a WEC simulation tool should

(a) be reliable for all possible trial vectors that an optimization algorithm might generate for evaluation (fidelity requirement).
(b) be general enough to be applicable to a wide variety of candidate WEC concepts (flexibility requirement) and,
(c) be fast/affordable enough to allow sufficient generations or iterations to be completed in practical time scales on available and affordable hardware (computational requirement).

LPF, and related approaches, scores very well in terms of the flexibility and computational requirements but have limitations in terms of fidelity. These limitations are due to the linearisation of the body boundary condition, linearisation of the water free surface boundary condition and also due to the invicid/irrotational assumptions inherent to all potential flow methods. The methods explored in this paper include methods that overcome two of these three difficulties, more specifically the methods are all potential flow methods but extend to nonlinear treatment of boundary conditions at the water free surface and the body surfaces.

1.2 Distinguishing characteristics of the wave energy problem

Potential flow and boundary integral methods are used widely in most, if not all, fields within offshore design and naval architecture. Historically, it is from these disciplines that wave energy research has emerged so it should not be surprising that wave energy also inherited a strong tradition in use of these methods. Nevertheless, wave energy has a number of characteristics that distinguish its analysis from that of other floating bodies. The ideal simulation tool for wave energy might not be the same as the ideal tool for analysis of a floating wind turbine, offshore platform or ship hull.

Floating platforms and ships are generally designed to minimise motion response to waves; in a small number of cases, this is accomplished through active systems but more typically it is done through optimisation of geometry and dynamic properties to minimise the response amplitude operator, at least in the predominant frequency range of the local waves. Conversely, WEC systems are designed to maximise wave interactions, at least with respect to power absorption. Most usually maximising power absorption also results in attracting very large wave forces and very large motion response amplitudes, at least in the power absorbing modes.

WEC devices are further distinguished by the presence of power take off (PTO) machinery and associated control systems. PTO systems are superficially similar to sub-systems present in other offshore systems, for example, gyroscopic

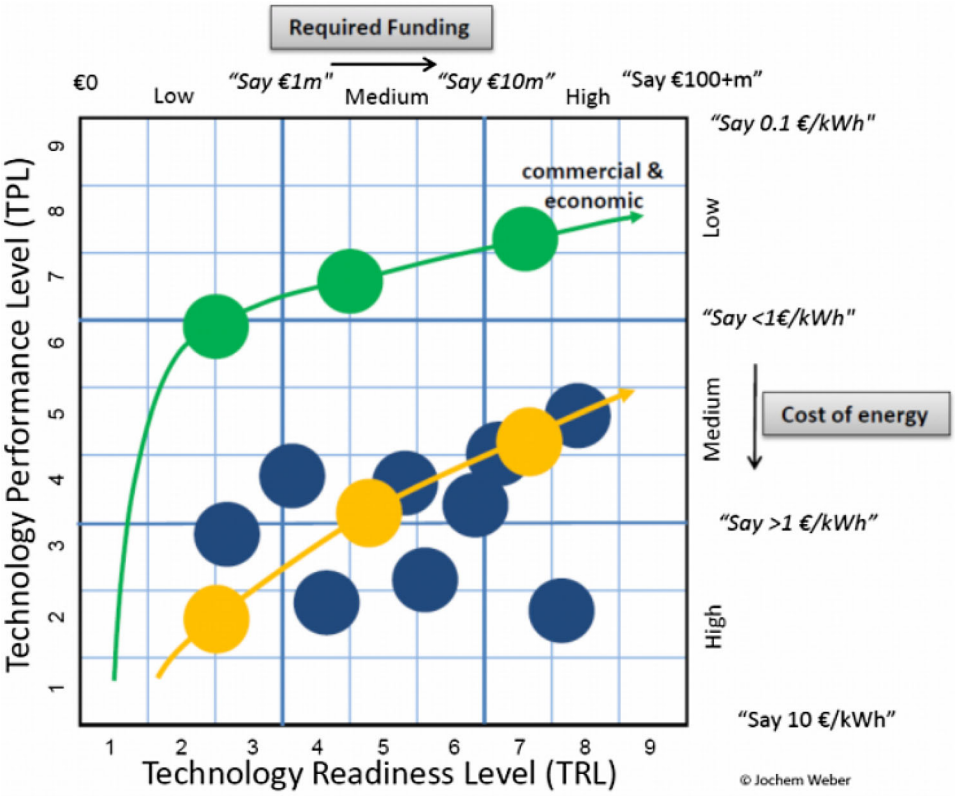

Fig. 1 TRL/TPL WEC development trajectories (Weber 2012)

ship stabilisation systems or crane heave compensation systems. These systems all introduce forces acting on floating bodies in addition to the wave forces. However, ship stabilisation or heave compensation systems generally reduce motion of the bodies that they act upon. WEC PTO systems, especially ones with advanced control systems, will tend to amplify the motion of the WEC bodies in response to waves. This is achieved through impedance matching, complex conjugate control, latching, unlatching or other approaches that manipulate the phase of the motion response so that the response velocity and wave forcing are in phase resulting in increased power and motion.

A first distinguishing characteristic of WEC systems is, therefore, increased response amplitudes when compared to other offshore structures in waves. It follows that that the assumptions made to allow linearisation of the boundary conditions are often invalidated in WEC simulations.

A second, techno-economic, distinguishing characteristic that separates WEC design from other offshore system design is that a minimum viable product has not yet been identified in WEC design whereas in other offshore design applications, a minimum viable product, and in many cases, multiple generations of incremental product improvements, has been demonstrated. The implication of this observation is that, in platform design and ship design, certain design approaches are known to work and we can be confident that the trade-offs, assumptions and imperfections in the analysis methodologies do not prevent production of a commercially successful design. It is necessary to search for more powerful design tools that reduce assumptions and trade-offs so that more insightful analysis is possible.

Mature general purpose software packages, both commercial and open source, exist for wave structure interaction and wave energy simulation. However, the theoretical and methodological underpinnings of these mature software packages encompass only a fraction of the breadth of the available methods that have been studied to date. Broadly speaking, these mature software packages are either LPF or RANS. Notwithstanding the extensive use that has been made of LPF and the potential of RANS in wave energy research, neither of these methods is ideal; LPF is fast but excludes important physical effects while RANS includes relevant physics but is too computationally demanding to be widely/solely applied in WEC design.

Boundary element methods, based on potential flow, have become a standard modelling tool for hydrodynamic modellers, both in industry and research laboratories. However, many are unaware of the range of modelling possibilities within the family of boundary element techniques, and the basis upon which these methods are formed is not always completely understood. As a result, many hydrodynamic modellers opt for the default case of linear potential methods, defined by Wehausen and Laitone (1960).

The objective of this paper is to review potential flow formulations that might play a part in next-generation WEC design tools. Of particular interest are potential flow formulations that are non-linear in the body boundary condition (if not all boundary conditions) and are free from "irregular frequencies". The work is a partnership between Wave Venture and the Centre for Ocean Energy Research at Maynooth University and is one of the number of early steps taken by Wave Venture in selecting the most appropriate theory for an advanced wave structure interaction model specially adapted to the needs of wave energy projects.

1.3 Previous reviews

Some hydrodynamic modelling reviews exist and cover a larger domain than boundary element methods, while generally focus on linear theory and second-order problems, such as those by Newman (2018), Faltinsen (1991), Ogilvie (1966) (for linear theory) or Ogilvie (1983) (for second-order). Some reviews do focus on specific applications, for example Beck and Reed (2001), but are not in the main application area of interest (zero speed) of this study. There are some broad-based reviews in the general application area of interest, such as Penalba et al. (2017), but without particular focus on potential flow, and lack detail on the methods employed. A wide variety of reviews exist on CFD modelling, e.g. Windt et al. (2018), but serve to accentuate the dearth of coverage of the area relating to potential flow. However, the review made by Yeung (1982) focuses on the theory for the different methods used to solve potential flow problems (boundary element method, finite difference and finite element method).

1.4 Outline of this paper

This paper presents a review of linear and non-linear potential flow models using the boundary element method for problems including a free-surface and bodies with no forward speed. Assumptions and equations leading to potential flow problems are treated. The linear theory at first order and the discretization of the problem by the panel method are presented. The two different methods used to solve the problem, respectively, the Green function method and Rankine sources are discussed, in both time and frequency domains, as well as the different existing approaches applied for the computation of the hydrodynamic forces exerted on a body. This paper reviews the linear and nonlinear numerical models that appeared since the 1970s thanks to the rapid development of numerical computation.

2 General equations

All the equations and software presented thereafter in this paper consider bodies as rigid bodies and do not include flexible bodies.

We consider the fixed right-handed coordinate system (x, y, z), with positive z vertically upwards through the center of gravity of the body and the origin in the plane of the undisturbed free-surface. The displacements at the center of gravity of the body in the x-, y-, and z-directions, with respect to the origin are x_G, y_G and z_G, respectively, so that x_G is surge, y_G is sway and z_G is the heave displacement. Let the angular displacements at the center of gravity of the body of the rotational motion about the x-, y-, and z-axes be α_r, β_r, γ_r.

Hence, to express the generalized body motion vector $X(t)$, we denote

$$X(t) = \begin{vmatrix} x_G \\ y_G \\ z_G \\ \alpha_r \\ \beta_r \\ \gamma_r \end{vmatrix}. \tag{1}$$

The assumptions of an incompressible, inviscid fluid and irrotational flow lead to a set of equations for potential flow theory, which, for a velocity potential ϕ and a free-surface elevation η, leads to

– the Laplace equation in the entire fluid domain (D)

$$\Delta\phi = 0, \tag{2}$$

– a kinematic free-surface boundary condition (no material flux across the free-surface) (on $z = \eta$)

$$\frac{\partial \eta}{\partial t} - \frac{\partial \phi}{\partial z} + \nabla\phi.\nabla\eta = 0, \tag{3}$$

– a dynamic free-surface boundary condition (Euler's integral, pressure on the free-surface elevation equal to the atmospheric pressure, where $P_{atm} = 0$ without loss in generality) (on $z = \eta$)

$$g\eta + \frac{\partial \phi}{\partial t} + \frac{1}{2}|\nabla\phi|^2 = 0, \tag{4}$$

– an impermeability condition on the seabed, with a unit normal vector to the surface n

$$\frac{\partial \phi}{\partial n} = 0, \tag{5}$$

– a body boundary condition (impermeability condition) for a body moving at a velocity V, with a normal n, on the wetted surface of the body

$$\frac{\partial \phi}{\partial n}(M,t) = V.n(M,t), \tag{6}$$

– a radiation condition, where the perturbed potential ϕ_p tends to 0 moving away from the body, where V is the velocity vector, the total potential ϕ is equal to the sum of an incident potential ϕ_0 and a perturbed potential ϕ_p

$$\phi = \phi_0 + \phi_p, \tag{7}$$

with Δ the Laplace operator, ∇ the gradient operator, ∂ the partial operator, g the acceleration due to gravity, and M any point in the fluid domain.

In the literature, different methods are proposed to solve the potential flow problem. Boundary element methods (BEMs), or panel methods, are based on the distribution of singularities (e.g., source) on the boundaries of the domain. The resulting equations are solved to obtain the source singularity strengths and, therefore, the velocity potentials. Other methods, such as finite difference methods (FDMs), finite volume methods (FVMs), or finite element methods (FEMs) are based on the discretization of the entire fluid domain where, in each node (or cell), the partial differential equations (PDE) of the problem are computed, either directly (FDM), or in their integral (FVM) or weak (FEM) formulation, depending on the particular method used. These three methods have significantly more unknowns than a BEM approach, since the entire fluid domain is discretised, but the matrix that must be inverted is very sparse, and the total computational effort and accuracy depends on the details of the code. The present study is only focused on BEM methods, largely employed in the field of wave–structure interactions.

Assuming incompressible and inviscid fluid, the governing Navier–Stokes equations evolve into Euler's equation. Progressively applying the assumption of irrotational flow leads to Euler's integral, giving access, knowing the velocity potential, to the pressure p

$$p = -\rho g z - \rho \frac{\partial \phi}{\partial t} - \frac{1}{2}\rho |\nabla \phi|^2, \tag{8}$$

where ρ is the water density.

The integration of the pressure gives the resulting hydrodynamic and hydrostatic forces (and moments) F_{hydro} acting on a surface (S) of normal n

$$F_{\text{hydro}} = -\iint_S p n \mathrm{d}s, \tag{9}$$

with the generalized unit normal vector n

$$n = \begin{vmatrix} n_1 \\ n_2 \\ n_3 \\ n_4 \\ n_5 \\ n_6 \end{vmatrix} = \begin{vmatrix} n_1 \\ n_2 \\ n_3 \\ \mathbf{y}n_3 - \mathbf{z}n_2 \\ \mathbf{z}n_1 - \mathbf{x}n_3 \\ \mathbf{x}n_2 - \mathbf{y}n_1 \end{vmatrix}. \tag{10}$$

Thus, applying Newton's second law, the equations of motion for a floating body can be expressed as

$$\mathbf{M}\ddot{X} = F_{\text{hydro}} - F_g + F_{\text{exter}}, \tag{11}$$

with

$$F_{g_3} = \mathbf{m}g, \tag{12}$$

where F_g is the gravitational force vector, $\mathbf{m}$ the mass of the body, $\mathbf{M}$ its mass matrix, and F_{exter} represents additional forces (due to mooring, PTO, etc.).

The potential can be represented in two different ways: by a mixed distribution of sources and dipoles over the domain boundaries (called the double-layer, or potential formulation), or by a distribution of sources only (also called the source formulation).

In the potential formulation, the potential outside the fluid domain (D) is assumed to be arbitrary. Green's second identity transforms a volumetric problem into an equivalent one on the boundary domain (S)

$$\begin{aligned} &\iiint_D (\phi(P)\Delta G(M,P) - G(M,P)\Delta\phi(P))\,\mathrm{d}D \\ &= \iint_S \left(\phi(P)\frac{\partial G(M,P)}{\partial n} - G(M,P)\frac{\partial \phi(P)}{\partial n}\right)\mathrm{d}S, \end{aligned} \tag{13}$$

with G a Green function, $P(a,b,c)$ a point where a source (or dipole) is placed, and $M(x,y,z)$ a point in the domain. The potential ϕ is itself a harmonic function that satisfies the Laplace equation in (2); therefore, the identity simplifies to

$$\begin{aligned} &\iiint_D \phi(P)\Delta G(M,P)\mathrm{d}D \\ &= \iint_S \left(\phi(P)\frac{\partial G(M,P)}{\partial n} - G(M,P)\frac{\partial \phi(P)}{\partial n}\right)\mathrm{d}S. \end{aligned} \tag{14}$$

Using Green's third identity, the volumetric integral term can be expressed as

$$\iiint_D \phi(P)\Delta G(M,P)\mathrm{d}D = -2\pi\phi(P), \tag{15}$$

which leads, with Eq. (14), to the boundary integral equation, for the potential formulation. On the boundaries S of the domain, the boundary integral equation is given by

$$2\pi\phi(M) + \iint_S \phi(P)\frac{\partial G}{\partial n}(M, P)\mathrm{d}S - \iint_S \frac{\partial \phi(P)}{\partial n}G(M, P)\mathrm{d}S = 0, \quad \text{on } S, \tag{16}$$

where the unknown potential can be interpreted as a distribution of sources and its derivative by a distribution of dipoles.

Alternatively, in the source formulation, when assuming that the potential inside and outside the domain are equal at the boundaries, the potential is expressed by a distribution of unknown sources of strength σ in the form

$$\phi(M) = \iint_S \sigma(P)G(M, P)\mathrm{d}P, \tag{17}$$

and Eq. (16) leads to the following integral equation:

$$\frac{\partial \phi}{\partial n}(M) = 2\pi\sigma(M) + \iint_S \sigma(P)\frac{\partial G(M, P)}{\partial n}\mathrm{d}S. \tag{18}$$

The potential and source formulations are very similar and both involve the same amount of computational effort. Usually, the potential formulation is preferred since it is more general and efficient, in particular with relatively thin elements. However, if the fluid velocity or second-order forces are required, the source formulation has an advantage, as it does not require the computation of the second derivatives of the Green function.

3 Discussion on existing models

In the field of potential flow theory, for water wave–body interaction problems, different numerical models have emerged over the last 50 years or so, thanks to advances in numerical computation. The biggest issues in solving potential flow problems lie in the computation of the nonlinear free-surface boundary condition equations, and in the treatment of the body boundary condition (in the case of freely moving bodies) which takes into account the relative motion between the moving body and the unsteady free-surface elevation. Different levels of assumption are made in the treatment of those conditions, which lead to more or less complex models (see Fig. 2). Unsurprisingly, a greater number of assumptions generally leads to mathematical problems which are easier to solve and faster numerical computation; however, the scope of validity will inevitably be reduced. The present study is focused on models based on boundary element methods, and do not cover the finite difference, finite volume, and finite element methods.

In the context of boundary element methods, a free-surface Green function or a Rankine source is used to simplify and transform a volumetric problem into a surface one. Strictly speaking, both the free-surface Green function and Rankine singularity are Green functions; however, for the sake of simplicity, in the present study, we will refer to the "free-surface Green function" by the shorter term"Green function". By construction, the Green function satisfies the linearized free-surface conditions and the radiation condition; hence, singularities are distributed only on the wetted surface of the body. This yields a significant computational reduction, but only waves with small steepness should be considered due to the linearisation of the free-surface. However, the analytical expression for the Green function is difficult to handle and has to be approximated. Moreover, the convolution product inside the Green function makes its computation time-consuming since it must be evaluated a large number of times. In the case of finite depth problems, the sea-bottom is assumed flat. The determination of the Green function is discussed in Sect. 5. The Rankine source is much easier to compute, but does not satisfy the free-surface conditions, which are approximated numerically by discretising the free-surface. Neither way is the radiation condition fulfilled, and has to be implemented either numerically, by the inclusion of a damping zone around the body, or via a hybrid method, where the Green function method, which satisfies the radiation condition, is used around the edges of the computational domain. Rankine sources are discussed in Sect. 6.

When solving potential flow problems which include a body, two problems have to be solved: the equation of the body motion and the equation of the fluid (potential flow problem), where both are linked by the hydrodynamic forces acting on the body. The solution of the problem takes different routes, depending on whether a Green function approach or Rankine sources are used. Likewise, problems which include fixed bodies (diffraction problem) or bodies undergoing prescribed or freely motion (radiation problem) must be treated differently. The different methods developed to compute hydrodynamic forces are presented in Sect. 7.

Across all the existing BEM models, the greatest level of simplification is achieved by considering the problem to be fully linear, by linearisation at the first-order of the free-surface and body boundary conditions. By considering waves with small steepness, and a free-surface elevation linearized around the plane $z = 0$, the free-surface conditions simplify into ordinary differential equations. Small body motion is assumed, and forces are computed on the mean wetted body surface. Linearisation allows the decomposition of the total potential into incident, diffraction and radiation potentials. Hydrostatic, Froude–Krylov, diffraction and radiation forces are assumed linear. Time-domain and frequency-domain representations are related via the Fourier transform.

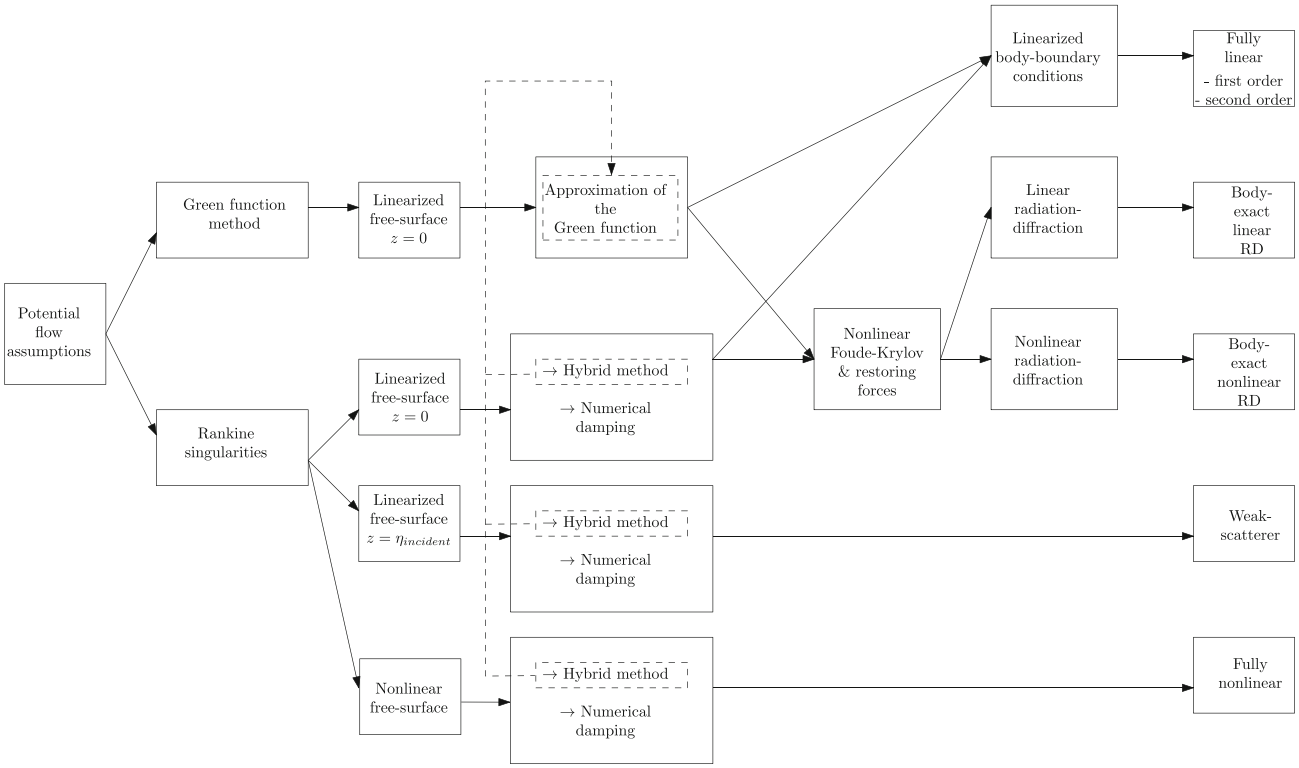

Fig. 2 Potential models in boundary element method

The first step to consider nonlinearities is to extend the linear model by computing second-order terms using a perturbation method. The second-order problem, in addition to extending the validity of the results, predicts some phenomena which cannot be accounted for, such as second-order effects forces and mean drift forces, by linear models.

A step towards the inclusion of nonlinearity is the use of the body-exact method. The main assumption is to assume that the body can undergo large motions in the presence of waves with small steepness. There are two versions of the body-exact method. In the first method, the concept, although inconsistent, consists of computing nonlinear Froude–Krylov (NLFK) and restoring forces on the instantaneous wetted surface of the body. The system becomes time varying and the link between time and frequency domains is, in principle, no longer available. However, the free-surface conditions remain linearized, and the linear diffraction–radiation forces are still computed on the mean wetted surface, and can be taken from a fully linear potential flow code. NLFK and restoring forces are computed by integration of the pressure on the exact wetted surface, and the position of the body is explicitly calculated (actualized) at each time step. The interface between the wetted surface and the free-surface elevation requires re-meshing of the body, which is time-consuming. However, taking into account the NLFK forces significantly improves the quality for the results for a relatively small increase in computation, under more significant body motion.

A second improvement of the body-exact method is to include nonlinearity related to the diffraction–radiation forces. Such an inclusion has a significant impact in the computation time of the Green function (or Rankine sources), which has to be re-evaluated at each time step.

All the models presented hitherto assume linear free-surface boundary conditions around the plane $z = 0$, and can be solved using the Green function or Rankine sources. The next level of complexity takes into the consideration full or partial nonlinearities of the free-surface conditions. The Green function, as explained before, can only deal with linearized free-surface equations, hence Rankine singularities are used in the following models.

The weak-scatterer approach that can be originally found in Pawlowski (1994) assumes that the perturbation potential is small compared to the incident one, and linearization of the free-surface elevation is made around the incident free-surface $z = \eta_0$. The main advantage of this method is that the incident wave is still known analytically and does not need to be propagated from a wave-maker, allowing the mesh to be refined only in the vicinity of the body.

The fully nonlinear model, which could be termed a numerical wave tank (NWT), does not make any particular assumptions and computes the fully nonlinear problem

with Rankine sources. The free-surface elevation is no longer known, and some instability in the computation of the free-surface elevation can appear. This method is very demanding in terms of computation time.

Nonlinearities can also be added in potential flow models by the inclusion of terms that take into account viscous effects, as the addition of drag forces. There are different ways to evaluate those forces, but the most popular remains the Morison's equation (can be found in Sarpkaya 1986). The inclusion of drag is beyond of the scope of the present review, and further details can be found in Ertekin and Rodenbusch (2016) (Section 35.1.6).

The linear potential flow model at first order, widely used in wave–structure interaction, is developed in Sect. 4. The nonlinear models (linear extended to second order, body exact, weak scatterer and fully nonlinear) are presented in Sect. 8.

Table 1 lists commercial and non-commercial potential codes which use the models described above. This non-exhaustive state-of-the-art overview highlights the different choices and techniques employed across different codes and gives a rough relative count of the codes available for the five potential models (fully linear, body exact linear/nonlinear radiation–diffraction, weak scatterer, and fully nonlinear). Codes dealing with any degree of nonlinearity are exclusively in the time domain, as hydrodynamic forces of a body undergoing sinusoidal motion become no longer simply sinusoidal. However, the LAMP code in Shin et al. (2003) is the only code to the best of the authors' knowledge that proposes a frequency-domain computation for large amplitude roll motion of a fishing vessel using the curve of statical stability (GZ curve), which leads to different responses for a given frequency. The two codes LAMP-4 and WS_Cn are weak-scatterer models, but both propose an option to consider linearized free-surface conditions, which lead to a body-exact nonlinear problem.

4 Linear potential flow theory

The free-surface boundary conditions (3) and (4) are difficult to implement numerically; hence, some linearisation is usually applied to the problem. The free-surface conditions (3) and (4) are highly nonlinear, and linearisation can be useful if considering small wave steepness. Assumptions are also usually made on the decomposition of the potential (7) and the body boundary condition (6).

4.1 Potential expression

Linearisation of the problem allows the decomposition of the perturbed potential expressed in (7) into a diffraction potential ϕ_{D} and a radiation potential ϕ_{R}:

$$\phi_p = \phi_{\mathrm{D}} + \phi_{\mathrm{R}}. \tag{19}$$

Hence, the total potential reduces to the sum of an incident potential, a diffraction potential and a radiation potential:

$$\phi = \phi_0 + \phi_{\mathrm{D}} + \phi_{\mathrm{R}}. \tag{20}$$

The incident and diffraction potentials correspond, respectively, to the potential created by the incident wave and the resulting wave, when the body is considered fixed. The radiation potential corresponds to the waves created by the motion of the body itself in the absence of the incoming waves.

4.2 Free-surface boundary conditions

Considering a linearized free-surface elevation of small steepness ϵ simplifies the free-surface boundary conditions:

– linearized kinematic free-surface boundary condition ($z = 0$):

$$\frac{\partial \eta}{\partial t} = \frac{\partial \phi}{\partial z}, \tag{21}$$

– linearized dynamic free-surface boundary condition ($z = 0$):

$$\eta = -\frac{1}{g}\frac{\partial \phi}{\partial t}, \tag{22}$$

which, by including (21) in (22), leads to

$$\frac{\partial^2 \phi}{\partial t^2} + g\frac{\partial \phi}{\partial z} = 0. \tag{23}$$

4.3 Body boundary conditions

On the linearized body boundary condition, forces are computed on the mean body wetted surface S_w:

$$\frac{\partial \phi}{\partial n}(M,t) = \frac{\partial \phi}{\partial n_0}(M,t) = V_0.n_0(M,t), \tag{24}$$

with V_0 velocity vector of the body, and n_0 normal of the body, at mean body position. Using the decomposition of the velocity potential, its derivative can be written as

$$\frac{\partial \phi}{\partial n} = \frac{\partial \phi_0}{\partial n} + \frac{\partial \phi_D}{\partial n} + \frac{\partial \phi_R}{\partial n}. \tag{25}$$

Considering the structure of the body boundary condition, a new decomposition of the radiation potential is introduced (see Newman 2018)

Table 1 Review of commercial and non-commercial wave–body interaction BEM codes

Model		$\frac{\text{Computation}}{\text{Simulation}}$	Code	Domain		Green function	Rankine source	
				Frequency	Time		Damping beach	Hybrid method
Fully linear		$o(1)$	LAMP-1 Shin et al. (2003)		x			x
			SWAN-1 Sclavounos and Nakos (1988)		x		x	
			WISH-1 Kim et al. (2011)		x		x	
			NEMOH Babarit and Delhommeau (2015)	x		x		
			WAMIT Version 7-0 (2013)	x		x		
			ACHIL3D Clément (1999a)		x	x		
			HYDROSTAR HydroStar Version 7-3 (2016)	x		x		
			AQUADYN Delhommeau (1993)	x		x		
			DIODORE Berhault et al. (1992)	x	x	x		
			NEWDRIFT Papanikolaou and Schellin (1992)	x		x		
			WADAM (2013)	x		x		
Body exact	Linear RD	$o(10)$	LAMP-2 Shin et al. (2003)		x			x
			SWAN-2 Sclavounos (1996)		x		x	
			WISH-2 Kim et al. (2011)		x		x	
			Gilloteaux (2010)		x	x		
			Liu and Papanikolaou (2011)		x			x
	NL	$o(10) - o(100)$	LAMP-4* Shin et al. (2003)		x			x
			WS_Cn* Letournel et al. (2018)		x		x	
Weak scatterer		$o(100)$	LAMP-4 Shin et al. (2003)		x			x
			SWAN-4 Huang (1997)		x		x	
			WISH-3 Kim et al. (2011)		x		x	
			WS_Cn Letournel et al. (2018)		x		x	
Fully nonlinear		$o(1000)$	Dombre et al. (2015)		x		x	
			Tanizawa (1995), Tanizawa and Minami (2001)		x		x	
			Cao et al. (1994)		x		x	
			Wu and Taylor (1996)		x		x	
			Koo and Kim (2004)		x		x	

The codes followed by the symbol * are codes originally implemented for a weak-scatterer model, with an option to consider linearized free-surface conditions. Names in italic correspond to the authors having developed their own non-commercial code

$$\phi_R = \sum_{i=1}^{6} V_i \phi_{Ri}, \tag{26}$$

with i representing one of the 6 degrees of freedom of the body, while the V_i are components of the generalized body velocity. The body boundary conditions can be written in a different way on the wetted surface S_w for the radiation and diffraction potentials, respectively (see Newman 2018),

$$\frac{\partial \phi}{\partial n} = \frac{\partial \phi_R}{\partial n} = \sum_{i=1}^{6} V_i n_i, \tag{27}$$

with

$$\frac{\partial \phi_{Ri}}{\partial n} = n_i, \tag{28}$$

and

$$\frac{\partial \phi_D}{\partial n} = -\frac{\partial \phi_0}{\partial n}. \tag{29}$$

A feature of this decomposition is that the potentials ϕ_0 and ϕ_D do not depend on the body motion.

4.4 Integral equations

Using Eq. (16) and the new linearized body boundary conditions (28) and (29), we obtain, respectively, the integral equations satisfied by the radiation and the diffraction velocity potential

$$2\pi\phi_{Ri}(M) + \iint_S \phi_{Ri}(P)\frac{\partial G(M,P)}{\partial n}\mathrm{d}S = \iint_S n_i G(M,P)\mathrm{d}S. \tag{30}$$

$$2\pi\phi_D(M) + \iint_S \phi_D(P)\frac{\partial G(M,P)}{\partial n}\mathrm{d}S = -\iint_S \frac{\partial \phi_0(P)}{\partial n} G(M,P)\mathrm{d}S. \tag{31}$$

The diffraction potential, given in (31), can also be written as follows:

$$2\pi\left[\phi_0(M) + \phi_D(M)\right] + \iint_S (\phi_0(P) + \phi_D(P))\frac{\partial G(M,P)}{\partial n} dS = 4\pi\phi_0(M). \tag{32}$$

From the computational point of view, (32) has some advantages over (31) in terms of computational time and storage space requirements.

4.5 Discretization

In the low-order potential formulation, the geometry is discretised with a number N of flat panels, where the velocity potential is assumed constant on each panel, and computed at a collocation point located at the center of the panel. The continuous integral equations, established in (30) and (32), can be reduced to a set of linear simultaneous equations for the values of the velocity potential over the panels. For the radiation potential, we obtain

$$2\pi\phi_{Ri}(M_j) + \sum_{k=1}^{N} \mathbf{D}_{jk}\phi_{Ri,k} = \sum_{k=1}^{N} \mathbf{S}_{jk} n_{i,k}, \tag{33}$$

with j and $k = 1, \ldots, N$. We obtain, for the diffraction potential,

$$2\pi\phi_D(M_j) + \sum_{k=1}^{N} \mathbf{D}_{jk}\phi_{D,k} = 4\pi\phi_0(M_j), \tag{34}$$

where the influence matrices $\mathbf{D}_{jk}$ and $\mathbf{S}_{jk}$ are defined by

$$\mathbf{D}_{jk} = \iint_{S_k} \frac{\partial G(P,M_j)}{\partial n}\mathrm{d}S_k, \tag{35}$$

$$\mathbf{S}_{jk} = \iint_{S_k} G(P,M_j)\mathrm{d}S_k, \tag{36}$$

where S_k denotes the surface of the kth panel.

In the source formulation given in (17), the potential is expressed by a distribution of sources only. In the low-order method, after discretization of the body surface with flat panels, with constant source strength on each panel, the potential is expressed by

$$\phi(M_j) = \sum_{k=1}^{N} \sigma(M_k) \iint_{S_k} G(M_j,P)\mathrm{d}S_k. \tag{37}$$

The linear system is composed of ordinary differential equations (33) and (34). A variety of algorithms exist to set the matrices and solve this resulting linear system of equations, but these algorithms do not have the same computational complexity, and have to be chosen depending on the size of the system.

4.6 Euler's integral

Euler's integral, established in (8), is linearized by neglecting quadratic terms, which leads to (on S_w)

$$p = p_s + p_d = -\rho g z - \rho\frac{\partial \phi}{\partial t}(M,t), \tag{38}$$

where p_s and p_d are the static and dynamic pressure, respectively, and gives the linearized expression for hydrostatic and hydrodynamic loads, F_H and F_i as

$$F_{Hi} = -\iint_{S_w} \rho g z n_{0i} \mathrm{d}s, \tag{39}$$

$$F_i = -\iint_{S_w} p_d n_{0i} \mathrm{d}s, \tag{40}$$

with n_{0i} the ith component of the unit normal vector of the body, at the mean body position. The hydrostatic loads can be written as the product of a hydrostatic restoring load matrix K_H and the body motion X

$$F_{Hi} = K_{Hij} X_j, \tag{41}$$

with the load exerted in direction i, due to a motion X in the j degree of freedom, and $K_{Hij} > 0$. The different methods to compute the hydrodynamic forces are given in Section 7. Further details on the computation of hydrostatic and hydrodynamic loads can be found in Aubault and Ertekin (2016) (Section 34.4.9).

5 The Green function

The determination of the Green function is a key to solve free-surface potential flow problems with linearized free-surface boundary conditions. Kellog expressed the generalized Green function for any potential flow problem in Kellogg (1954) (p. 236):

$$G(M, P) = \frac{1}{r} + W(M, P), \tag{42}$$

where W is a harmonic function and r is the distance between the two points M and P. The theory of the Green function for free-surface flow problems can be found in the books of Stoker (1957) and Wehausen and Laitone (1960), as well as John (1950) for the frequency-domain Green function, and Finkelstein (1957) in the case of the transient Green function.

5.1 Determination of the Green function in the frequency domain

Let $\mathbf{g}$ be a potential, $\mathbf{g}_1 = \Re(\mathbf{g})$ its real part, and $\mathbf{g}_2 = \Im(\mathbf{g})$ its imaginary part

$$\mathbf{g}(x, y, z) = \mathbf{g}_1(x, y, z) + i\mathbf{g}_2(x, y, z). \tag{43}$$

We consider a source of pulsating strength (see Wehausen and Laitone 1960, Section 13) in three dimensions, at the position (a, b, c) defined for $z \leq 0$ by

$$\begin{aligned} G(x, y, z, t) &= \mathbf{g}_1(x, y, z)\cos(\omega t) + \mathbf{g}_2(x, y, z)\sin(\omega t) \\ &= \Re\left[\mathbf{g}(x, y, z)e^{-i\omega t}\right]. \end{aligned} \tag{44}$$

Laplace equation The potential $\mathbf{g}$ satisfies the Laplace equation

$$\Delta\mathbf{g} = \frac{\partial^2 \mathbf{g}}{\partial x^2} + \frac{\partial^2 \mathbf{g}}{\partial y^2} + \frac{\partial^2 \mathbf{g}}{\partial z^2} = 0. \tag{45}$$

Linearized free-surface condition $\mathbf{g}$ is a harmonic function of the time; therefore, the linearized free-surface condition (21) and the equation of the free-surface elevation (22) become

$$\frac{\partial \mathbf{g}_i}{\partial z}(x, y, 0) - \frac{\omega^2}{g}\mathbf{g}_i(x, y, 0) = 0, \tag{46}$$

and

$$\eta(x, y, t) = \frac{\omega}{g}\left[\mathbf{g}_1(x, y, 0)\sin(\omega t) - \mathbf{g}_2(x, y, 0)\cos(\omega t)\right], \tag{47}$$

for $i = 1, 2$.

Condition at infinite depth $(z \to \infty)$ We assume the separation of the variable z from $\mathbf{g}(x, y, z)$

$$\mathbf{g}(x, y, z) = Z(z)\mathbf{g}(x, y), \tag{48}$$

with Z a function depending on the variable z only. The Laplace equation can then be written as

$$\Delta\mathbf{g}(x, y) + m^2\mathbf{g}(x, y) = 0, \quad Z'' - m^2 Z = 0. \tag{49}$$

Three cases lead to different solutions: $m^2 > 0, m^2 < 0$, and $m^2 = 0$. We assume that the potential of outgoing waves is periodic in space along (x, y). Hence, only the case $m^2 > 0$ is treated, and $Z(z)$ is given by

$$Z = Ae^{mz} + Be^{-mz}, \tag{50}$$

with A and B constants. If the fluid is infinitely deep, $\frac{\partial \mathbf{g}}{\partial z}(x, y, z)$ must remain bounded as $z \to \infty$; hence, the term B must be 0. Moreover, the free-surface condition (46) requires the dispersion relation

$$m = k_0 = \frac{\omega^2}{g}, \tag{51}$$

with k_0 being the wave number. $\mathbf{g}(x, y, z)$ is of the form

$$\mathbf{g}(x, y, z) = e^{k_0 z}\mathbf{g}(x, y), \tag{52}$$

which implies, for a fluid of infinite depth, the following condition:

$$\lim_{z\to\infty}\frac{\partial \mathbf{g}_i}{\partial z}=0, \tag{53}$$

for $i=1,2$.

Condition at the sea-bottom in finite depth ($z=-h$) When the fluid is of finite depth h, the sea-bottom is assumed flat and the no flux condition is given by

$$\frac{\partial G}{\partial z}(x,y,-h)=0. \tag{54}$$

Considering the sea-bottom condition, and the separation of variables made in (48), Eq. (50) becomes

$$Z=A\cosh[m(z+h)], \tag{55}$$

and the free-surface boundary condition (46) becomes

$$m\tanh(mh)=k_0, \tag{56}$$

with two real solutions $\pm m_0$ (the solution $m_0<0$ is, however, meaningless in the present set of problems). $\mathbf{g}$ then takes the form

$$\mathbf{g}(x,y,z)=\cosh[m_0(z+h)]\mathbf{g}(x,y). \tag{57}$$

Radiation condition at infinite distance ($r\to\infty$) As the potential behaves like outgoing waves in the far field, a radiation condition is imposed using a condition of the type of the Sommerfeld radiation condition, given by

$$\lim_{r\to\infty}\sqrt{r}\left(\frac{\partial \mathbf{g}}{\partial r}-ik_0\mathbf{g}\right)=0, \tag{58}$$

with $r^2=(x-a)^2+(y-b)^2+(z-c)^2$.

Determination of the Green function in infinite depth We wish to find a function satisfying conditions (45), (46), (58), and particularly for the case of infinite depth case equation (53). We assume the Green function G to be

$$G(x,y,z,t)=\left[\frac{1}{r}+\mathbf{g}_0(x,y,z)\right]\cos(\omega t)+\mathbf{g}_2(x,y,z)\sin(\omega t). \tag{59}$$

The term $\frac{1}{r}$ is the fundamental free-space Green function, and $\mathbf{g}_0$ is the free-surface term. $\mathbf{g}_2$ will be determined at the end to satisfy the radiation condition (58). Using the double Fourier transform in polar coordinates $(k,\theta,z,)$ $\frac{1}{r}$ and $\mathbf{g}_0$ can be written

$$\frac{1}{r}=\frac{1}{2\pi}\int_0^\infty\int_{-\pi}^{\pi}\mathrm{e}^{-k|z-c|}e^{ik[(x-a)\cos\theta+(y-b)\sin\theta]}\mathrm{d}\theta\mathrm{d}k, \tag{60}$$

$$\mathbf{g}_0(x,y,z)=\frac{1}{2\pi}\int_0^\infty\int_{-\pi}^{\pi}\hat{\mathbf{g}}_0(k,\theta,z)\,\mathrm{e}^{ik(x\cos\theta+y\sin\theta)}\mathrm{d}\theta\mathrm{d}k. \tag{61}$$

Applying the Laplace equation (45) and the double Fourier transform, we have

$$\frac{\partial^2\hat{\mathbf{g}}_0}{\partial z^2}-k\hat{\mathbf{g}}_0=0. \tag{62}$$

In infinite depth, using the approach leading to (52) we find

$$\hat{\mathbf{g}}_0(k,\theta,z)=A_0(k,\theta)e^{kz}. \tag{63}$$

Considering the Fourier transforms (60) and (61), one can compute the term A_0 with equation (46)

$$A_0(k,\theta)=\frac{k+k_0}{k-k_0}e^{kc}e^{-ik[a\cos\theta+b\sin\theta]}\mathrm{d}\theta\mathrm{d}k. \tag{64}$$

Hence, we have

$$\mathbf{g}_0(x,y,z)=\frac{1}{2\pi}\times\int_0^\infty\int_{-\pi}^{\pi}\frac{k+k_0}{k-k_0}\mathrm{e}^{k(z+c)}\mathrm{e}^{ik[(x-a)\cos\theta+(y-b)\sin\theta]}\mathrm{d}\theta\mathrm{d}k. \tag{65}$$

A singularity appears at $k=k_0$, so the potential is expressed as Cauchy principal value integral

$$\mathbf{g}_1(x,y,z)=\frac{1}{r}+\frac{1}{2\pi}PV\int_0^\infty\times\int_{-\pi}^{\pi}\frac{k+k_0}{k-k_0}\mathrm{e}^{k(z+c)}\mathrm{e}^{ik[(x-a)\cos\theta+(y-b)\sin\theta]}\mathrm{d}\theta\mathrm{d}k. \tag{66}$$

Introducing the zero-order Bessel function of the first kind

$$J_0(kR)=\frac{1}{2\pi}\int_{-\pi}^{\pi}\mathrm{e}^{-ikR\sin\alpha}\mathrm{d}\alpha, \tag{67}$$

and considering the polar coordinates

$$x-a=R\cos\alpha,\quad y-b=R\sin\alpha,\quad R^2=(x-a)^2+(y-b)^2 \tag{68}$$

one can write

$$\mathbf{g}_1(R,\alpha,\theta)=\frac{1}{r}+\frac{1}{r_1}$$

$$+2k_0 PV\int_0^\infty \frac{1}{k-k_0}\mathrm{e}^{k(z+c)}J_0(kR)\mathrm{d}k, \tag{69}$$

with $r_1^2=(x-a)^2+(y-b)^2+(z+c)^2$. Regarding the behavior of $\mathbf{g}_1$ at infinite distance, we can obtain an asymptotic expression modifying the order of integration and making a change of variable ($\theta\to\Omega$) in (66)

$$\begin{aligned}\mathbf{g}_1(x,y,z)&=\frac{1}{r}+\frac{1}{r_1}\\&\quad+\frac{k_0}{\pi}PV\int_0^\infty\int_{-\pi}^{\pi}\frac{1}{k-k_0}\mathrm{e}^{k(z+c)}\mathrm{e}^{ikR\cos(\theta-\alpha)}\mathrm{d}\theta\mathrm{d}k,\\&=\frac{1}{r}+\frac{1}{r_1}\\&\quad+\frac{4k_0}{\pi}PV\int_0^\infty\int_0^{\frac{\pi}{2}}\frac{1}{k-k_0}\mathrm{e}^{k(z+c)}\cos(kR\cos\theta)\mathrm{d}\theta\mathrm{d}k,\\&=\frac{1}{r}+\frac{1}{r_1}\\&\quad+\frac{4k_0}{\pi}PV\int_0^\infty\int_0^1\frac{1}{\sqrt{1-\Omega^2}}\\&\quad\times\frac{1}{k-k_0}\mathrm{e}^{k(z+c)}\cos(kR\Omega)\mathrm{d}\Omega\mathrm{d}k.\end{aligned} \tag{70}$$

Considering the following relation

$$\begin{aligned}\cos(kR\Omega)&=\cos(k_0R\Omega)\cos[(k-k_0)R\Omega]\\&\quad-\sin(k_0R\Omega)\sin[(k-k_0)R\Omega],\end{aligned} \tag{71}$$

and using the theorem from Fourier integrals (discussed in Bochner 1948)

$$\begin{aligned}\int_a^\infty f(x)\frac{\sin[R(x-x_0)]}{x-x_0}\mathrm{d}x&=\pi f(x_0)+o\left(\frac{1}{R}\right),\\PV\int_a^\infty f(x)\frac{\cos[R(x-x_0)]}{x-x_0}\mathrm{d}x&=o\left(\frac{1}{R}\right),\end{aligned} \tag{72}$$

we can then write

$$\begin{aligned}\mathbf{g}_1(x,y,z)&=-4k_0\mathrm{e}^{(z+c)}\int_0^1\frac{1}{\sqrt{1-\Omega^2}}\sin(k_0R\Omega)\\&\quad+o\left(\frac{1}{R}\right).\end{aligned} \tag{73}$$

This asymptotic expansion is known and can be found in Erdélyi (1956). It is given by

$$\begin{aligned}\mathbf{g}_1(x,y,z)&=-2\pi k_0\mathrm{e}^{k_0(z+c)}\sqrt{\frac{2}{\pi k_0R}}\sin\left(k_0R-\frac{\pi}{4}\right)\\&\quad+o\left(\frac{1}{R}\right).\end{aligned} \tag{74}$$

To take into account the radiation condition (58), $\mathbf{g}_2$ must have the asymptotic behavior

$$\begin{aligned}\mathbf{g}_2(x,y,z)&=2\pi k_0\mathrm{e}^{k_0(z+c)}\sqrt{\frac{2}{\pi k_0R}}\cos\left(k_0R-\frac{\pi}{4}\right)\\&\quad+o\left(\frac{1}{R}\right).\end{aligned} \tag{75}$$

The zero-order Bessel function of the first kind has the following asymptotic expansion (can be found in Watson (1924))

$$J_0(k_0R)=\sqrt{\frac{2}{\pi k_0R}}\sin\left(k_0R-\frac{\pi}{4}\right)+o\left(\frac{1}{R}\right), \tag{76}$$

when $R\to\infty$, and also satisfies (45), (46), and (53). We can then write $\mathbf{g}_2$ as

$$\mathbf{g}_2(x,y,z)=2\pi k_0\mathrm{e}^{k_0(z+c)}J_0(k_0R). \tag{77}$$

Therefore, we can express the complete potential, similar to Wehausen and Laitone (1960), (Eq. 13.17)

$$\begin{aligned}G(x,y,z,t)&=\left[\frac{1}{r}+\frac{1}{r_1}+2k_0PV\int_0^\infty\frac{1}{k-k_0}\mathrm{e}^{k(z+c)}J_0(kR)\mathrm{d}k\right]\\&\cos(\omega t)+2\pi k_0\mathrm{e}^{k_0(z+c)}J_0(k_0R)\sin(\omega t).\end{aligned} \tag{78}$$

The first term $1/r$ is called a Rankine source and $1/r_1$ is its image, reflected in the plane $z=0$. These two terms correspond to the free-space part of the Green function. One can also write the potential as

$$\begin{aligned}G(x,y,z,t)&=\left[\frac{1}{r}+PV\int_0^\infty\frac{k+k_0}{k-k_0}\mathrm{e}^{k(z+c)}J_0(kR)\mathrm{d}k\right]\\&\times\cos(\omega t)+2\pi k_0\mathrm{e}^{k_0(z+c)}J_0(k_0R)\sin(\omega t),\end{aligned} \tag{79}$$

or, in its complex form, as

$$\begin{aligned}\mathbf{g}(x,y,z)&=\frac{1}{r}+PV\int_0^\infty\frac{k+k_0}{k-k_0}\mathrm{e}^{k(z+c)}J_0(kR)\mathrm{d}k\\&\quad+i2\pi k_0\mathrm{e}^{k_0(z+c)}J_0(k_0R).\end{aligned} \tag{80}$$

Another way to express the potential is to change the path of integration, using contour integration, to remove the singularity at $k=k_0$, as Havelock (1955) did

$$\begin{aligned}\mathbf{g}(x,y,z)&=\frac{1}{r}+\frac{1}{r_1}+\frac{4k_0}{\pi}\int_0^\infty[k_0\cos[k(z+c)]\\&\quad-k\sin[k(z+c)]]\frac{K_0(kR)}{k^2+k_0^2}\mathrm{d}k\\&\quad-2\pi k_0\mathrm{e}^{k_0(z+c)}Y_0(k_0R)\\&\quad+i2\pi k_0\mathrm{e}^{k_0(z+c)}J_0(k_0R),\end{aligned} \tag{81}$$

where Y_0 is the zero-order Bessel function of the second kind, and K_0 the zero-order modified Bessel function of the second kind. Another representation is proposed by Kim (1965), using the Struve function of order zero $\mathbf{H}_0$:

$$\mathbf{g}(x,y,z) = \frac{1}{r} + \frac{1}{r_1} - \pi k_0 \mathrm{e}^{k_0(z+c)} \times \left(\mathbf{H}_0(k_0 R) + Y_0(k_0 R) - 2i J_0(k_0 R) + \frac{2}{\pi} \int_{z+c}^{0} \frac{\mathrm{e}^{-k_0 k}}{\sqrt{R^2+k^2}} \mathrm{d}k \right). \tag{82}$$

Determination of the Green function in finite depth We now consider a fluid of finite depth h. The potential satisfies conditions (45), (46), (58), and particularly for the case of finite depth case Eq. (54). We assume the given potential to be

$$G(x,y,z,t) = \left[\frac{1}{r} + \frac{1}{r_2} + \mathbf{g}_0(x,y,z) \right] \cos(\omega t) + \mathbf{g}_2(x,y,z) \sin(\omega t), \tag{83}$$

with

$$r_2^2 = (x-a)^2 + (y-b)^2 + (z+2h+c)^2. \tag{84}$$

Equation (63) becomes

$$\hat{\mathbf{g}}_0(k,\theta,z) = A_0(k,\theta) \cosh[k(z+h)], \tag{85}$$

with

$$A_0(k,\theta) = \frac{2(k+k_0)\mathrm{e}^{-kh} \cosh[k(c+h)]}{k \sinh(kh) - k_0 \cosh(kh)} \mathrm{e}^{-ik(a\cos\theta + b\sin\theta)}, \tag{86}$$

which gives the final expression for the potential, in finite depth, as

$$G(x,y,z) = \left[\frac{1}{r} + \frac{1}{r_2} + PV \int_0^\infty \times \frac{2(k+k_0)\mathrm{e}^{-kh} \cosh[k(c+h)] \cosh[k(z+h)]}{k \sinh(kh) - k_0 \cosh(kh)} J_0(kR)\mathrm{d}k \right] \cos(\omega t) + \frac{2\pi(m_0+k_0)\mathrm{e}^{-m_0 h} \sinh(m_0 h) \cosh[m_0(c+h)] \cosh[m_0(z+h)]}{k_0 h + \sinh^2(m_0 h)} \times J_0(m_0 R) \sin(\omega t). \tag{87}$$

with

$$m_0 \tanh(m_0 h) = k_0, \tag{88}$$

and

$$\frac{\mathrm{e}^{-m_0 h} \sinh(m_0 h)}{k_0 h + \sinh^2(m_0 h)} = \frac{m_0 - k_0}{m_0^2 h - k_0^2 h + k_0}. \tag{89}$$

John (1950) first derived a variety of representations of both infinite and finite water depth, and proposed an eigenfunction expansion in finite depth,

$$G(x,y,z) = 2\pi \frac{k_0^2 - m_0^2}{h m_0^2 - h k_0^2 + k_0} \cosh[m_0(z+h)] \times \cosh[m_0(c+h)] [Y_0(m_0 R)\cos(\omega t) - J_0(m_0 R)\sin(\omega t)] + 4 \sum_{k=1}^{\infty} \frac{m_k^2 + k_0^2}{h m_k^2 + h k_0^2 - k_0} \cos[m_k(z+h)] \times \cos[m_k(c+h)] K_0(m_k R)\cos(\omega t) \tag{90}$$

with m_k, $k > 0$ as the positive real roots of the equation $m_k \tanh(m_k) = -k_0$. Newman (1985) considered the expansion of (90) to be numerically efficient when $R/h > 0.5$ but, when the ratio R/h gets smaller, it becomes useless since each summand contains a logarithmic singularity when $R/h = 0$.

5.2 Determination of the Green function in the time domain

In this section, we determine, for both finite and infinite depth, the transient (or time-domain) Green function for the diffraction–radiation problem. The approach used here for the infinite depth case is that employed by Wehausen and Laitone (1960). Finkelstein (1957) describes accurately the construction of the time-domain Green function. We consider a source of variable strength $\zeta(t)$ at a position $P(a(t), b(t), c(t))$, starting from rest ($\zeta = 0$ for $t < 0$), in three dimensions (see Wehausen and Laitone (1960), Section 13.), defined for $z \leq 0$, and satisfying the following conditions:

$$\Delta G = 0, \tag{91}$$

$$\frac{\partial^2 G}{\partial t^2}(x,y,0,t) + g \frac{\partial G}{\partial z}(x,y,0,t) = 0, \tag{92}$$

$$\frac{\partial G}{\partial z}(x,y,-h) = 0 \text{ if } z = -h, \text{ or } \lim_{z\to\infty} \frac{\partial G}{\partial z} = 0, \tag{93}$$

$$\lim_{R\to\infty} \frac{\partial G}{\partial R} = 0, \tag{94}$$

$$G(x,y,0,0) = \frac{\partial G}{\partial t}(x,y,0,0) = 0. \tag{95}$$

In infinite depth We assume the given potential (see Finkelstein 1957, Appendix, and Wehausen and Laitone (1960), p.

491) to be of the form

$$G = \frac{\zeta}{r} - \frac{\zeta}{r_1} + G_1, \tag{96}$$

with $r_1^2 = (x-a)^2 + (y-b)^2 + (z+c)^2$, and G_1 harmonic in $z < 0$ satisfying conditions (93), (94), (95), and

$$\frac{\partial^2 G_1}{\partial t^2}(x, y, 0, t) + g\frac{\partial G_1}{\partial z}(x, y, 0, t) = \frac{-2g\zeta c}{\sqrt[3/2]{(x-a)^2 + (y-b)^2 + c^2}}, \quad t \geq 0. \tag{97}$$

Taking the Laplace transform of G_1

$$\bar{G}_1(x, y, z, s) = \int_0^\infty e^{-st} G_1(x, y, z, t)\mathrm{d}t, \tag{98}$$

we can then write (97) in the Laplace domain

$$s^2\bar{G}_1(x, y, 0, s) + g\frac{\partial \bar{G}_1}{\partial z}(x, y, 0, s) = -2g\int_0^\infty \mathrm{e}^{-st}\frac{\zeta c}{\sqrt[3/2]{(x-a)^2 + (y-b)^2 + c^2}}\mathrm{d}t. \tag{99}$$

We can extend (99) over the complete ($\forall z$) domain, as

$$s^2\bar{G}_1(x, y, z, s) + g\frac{\partial \bar{G}_1}{\partial z}(x, y, z, s) = -2g\int_0^\infty \mathrm{e}^{-st}\frac{\zeta(z+c)}{\sqrt[3/2]{(x-a)^2 + (y-b)^2 + (z+c)^2}}\mathrm{d}t, \tag{100}$$

as the equation is harmonic for $z < 0$ and satisfies conditions (94) and (95). Using the transform (60), we obtain

$$\begin{aligned} &s^2\bar{G}_1(x, y, z, s) + g\frac{\partial \bar{G}_1}{\partial z}(x, y, z, s) \\ &= \frac{g}{\pi}\int_0^\infty k\int_0^\infty \mathrm{e}^{-st}\zeta(t)\mathrm{e}^{k(z+c)} \\ &\quad\times\int_{-\pi}^{\pi}\mathrm{e}^{ik[(x-a)\cos\theta+(y-b)\sin\theta]}\mathrm{d}\theta\mathrm{d}t\mathrm{d}k, \\ &= 2g\int_0^\infty k\int_0^\infty \mathrm{e}^{-st}\zeta(t)\mathrm{e}^{k(z+c)}J_0(kR)\mathrm{d}t\mathrm{d}k, \end{aligned} \tag{101}$$

which leads to the solution

$$\bar{G}_1(x, y, z, s) = 2g\int_0^\infty \frac{k}{s^2 + gk}\int_0^\infty \mathrm{e}^{-st}\zeta(t)\mathrm{e}^{k(z+c)}J_0(kR)\mathrm{d}t\mathrm{d}k. \tag{102}$$

Using the convolution theorem, and the fact that $\frac{1}{s^2+gk}$ is the transform of $\frac{\sin(\sqrt{gk}t)}{\sqrt{gk}}$, we can find

$$G_1(x, y, z, t) = 2\int_0^\infty \sqrt{gk}\int_0^t \sin\left[\sqrt{gk}(t-\tau)\right]\zeta(\tau)\mathrm{e}^{k(z+c(\tau))}J_0(kR(\tau))\mathrm{d}\tau\mathrm{d}k. \tag{103}$$

For fixed t, and using properties of the Fourier–Bessel transform defined in Watson (1924), we can find that G_1 is $O(R^{-\frac{1}{2}})$, and therefore, satisfies condition (95). One can now write the complete expression for the potential G, similar to Wehausen and Laitone (1960) (Eq. 13.49)

$$G(x, y, z, t) = \frac{\zeta(t)}{r(t)} - \frac{\zeta(t)}{r_1(t)} + 2\int_0^\infty \sqrt{gk} \times\int_0^t \sin\left[\sqrt{gk}(t-\tau)\right]\zeta(\tau)\mathrm{e}^{k(z+c(\tau))}J_0(kR(\tau))\mathrm{d}\tau\mathrm{d}k. \tag{104}$$

In their theses, Liapis (1986) and later King (1987) do not use the integrated form obtained in (104), but the impulse response function form of the Green function

$$G(x, y, z, t) = \left(\frac{1}{r} - \frac{1}{r_1}\right)\delta(t-\tau) + 2H(t-\tau)\int_0^\infty \sqrt{gk}\sin(\sqrt{gk}(t-\tau))\mathrm{e}^{k(z+c)}J_0(kR)\mathrm{d}k. \tag{105}$$

As obtained in the frequency-domain (78), the first two terms are the free-space part of the Green function. The integral term, which includes a convolution product, corresponds to the memory part of the Green function. $\delta(t-\tau)$ is the Dirac delta function, and H the Heaviside step function given by

$$H(t-\tau) = \int_{-\infty}^t \delta(t-\tau)\mathrm{d}\tau. \tag{106}$$

The potential expressed in (105) represents the potential at a point (x, y, z) and time t due to an impulsive disturbance at the point (a, b, c) suddenly created and annihilated at time τ. The time is integrated later in the calculation, with respect to τ, from 0 to t.

In finite depth For the finite depth case, Wehausen and Laitone (1960) (Eq. 13.53) give the expression for the transient Green function, for a potential of strength $\zeta(t)$ in a fluid of depth h

$$G(x, y, z, t) = \frac{\zeta(t)}{r} + \frac{\zeta(t)}{r_2} - 2\zeta(t)\int_0^\infty \mathrm{e}^{-kh}\frac{\cosh[k(c(t)+h)]\cosh[k(z+h)]}{\cosh kh}J_0(kR(t))\mathrm{d}k$$

$$+2\int_0^\infty\int_0^t \zeta(\tau)\frac{\cosh[k(c(\tau)+h)]\cosh[k(z+h)]}{\cosh^2(kh)\sqrt{\tanh(kh)}} \times\sqrt{gk}\sin\left[(t-\tau)\sqrt{gk\tanh(kh)}\right]J_0(kR(\tau))\mathrm{d}\tau\mathrm{d}k, \quad (107)$$

with

$$r_2^2=(x-a)^2+(y-b)^2+(z+2h+c)^2. \quad (108)$$

The approach to calculate expression (107) is explained further in detail in the works of Finkelstein (1957), and Lunde (1951). In his work, to approximate the transient Green function in finite depth, Newman (1992) uses the impulse response form of the Green function

$$G(x,y,z,t)=\left(\frac{1}{r}+\frac{1}{r_2} -2\int_0^\infty \mathrm{e}^{-kh}\frac{\cosh[k(c+h)]\cosh[k(z+h)]}{\cosh kh}J_0(kR)\mathrm{d}k\right) \times\delta(t-\tau)+2H(t-\tau)\int_0^\infty\frac{\cosh[k(c+h)]\cosh[k(z+h)]}{\cosh^2(kh)\sqrt{\tanh(kh)}} \times\sqrt{gk}\sin[(t-\tau)\sqrt{gk\tanh(kh)}]J_0(kR)\mathrm{d}k. \quad (109)$$

5.3 Approximation of the Green function and its derivatives

Many studies have considered the approximation of the free-surface Green function for zero-forward speed diffraction–radiation problems, in both the time and frequency domains, for both finite and infinite water depth. Here, we discuss the different models developed in the literature, and their relative efficiency. As the Green function is evaluated for each panel, for each body geometry, and at each frequency (in the frequency domain), the development of algorithms which provide good accuracy and short computation cost is crucial.

5.3.1 Approximation in the frequency domain

Infinite depth approximation Newman (1985) first proposed an algorithm to compute the Green function and its derivatives in the frequency domain for both finite and infinite depth cases, giving accurate results. The domain is separated into different sub-domains and approximated by rational polynomials and Chebyshev polynomials. The Green function and its first derivative are evaluated simultaneously with accuracy to six decimal places. The computation for the finite depth case is around six times slower than for infinite depth, due to its greater complexity. Newman's algorithm is used in the boundary integral method (BIM) code WAMIT Version 7-0 (2013).

Later, Telste and Noblesse (1986) published a numerical method based on Noblesse's (1982) previous study to evaluate the Green function (and its derivatives) in deep water. The method consists of dividing the single integral obtained in (78) into 'near-field' and 'far-field' integrals. Similar to Newman's method, the domain is divided into five sub-domains for the approximation.

Delhommeau (1989) proposed a fast method to compute the Green function and its derivatives, using numerical interpolation across files of four tabulated functions. A tabulation method is used for near and moderate fields, while asymptotic expressions are used for the far field. Delhommeau's algorithm is used in the code (Babarit and Delhommeau 2015).

Linton and McIver (2001), and later Peter and Meylan (2004), proposed a derivation of John's eigenfunction representation (90) for the infinite depth Green function. The eigenfuncion expansion is more numerically efficient than other approaches, but works on the assumption of axial symmetry. Linton's method can be useful when using hybrid methods which employ both Rankine and Green functions, discussed in Sect. 6.4.2.

Clément (2013) proposed a second-order ordinary differential equation (ODE) to solve infinite depth water problems. A study led by Xie et al. (2018a), Xie (2019) showed that solving the ODE is more practical, more efficient and faster than evaluating integrals in the frequency domain. Clement's approach is very efficient compared to the classical Newman's approach showing that the ODE method is around 200 times faster for similar accuracy.

Wu et al. (2017) proposed a global approximation for deep water problems, decomposing the Green function and its gradient using a free-space singularity, specifically a non-oscillatory local-flow component, for which simple global approximations using elementary function are valid within the entire flow region, and wave components involving the Bessel function. These global analytical approximations are particularly simple and well suited for parallel computations, since they avoid the 'if' statements that are required where different approximations are used for different sub-domains.

A complete overview of the different analytical expressions for the Green function used in the literature, and a comparison of different approximations between the methods of Newman, Telste–Noblesse, Delhommeau, and Wu et al. has been reported by Xie et al. (2018b), for infinite depth problems. A conclusion of this article is that the most accurate approach is Newman's algorithm with 6 decimal place accuracy (DA), but it is also the slowest (10^-7 s average computation time (ACT)). The fastest method is that implemented by Wu, with 10^-9 s ACT, but less accurate with only 3 DA. The Telste–Noblesse algorithm is a good compromise (compared to Delhommeau's) between Wu and Newman, with 5 DA and 10^-8 s ACT.

Recently, Wu et al. (2018) updated their method by modifying the evaluation of the wave component term of the Green function. A new comparison of this model would be interesting to see, concerning relative accuracy, and should also include Clément ODE method (Clément 2013), which showed promising results, with 6 DA and $10^{-}9$ s ACT.

Finite depth approximation In the case of finite depth problems, the evaluation of the Green function and its derivative is more complicated, due to the complexity of the Green function. Newman (1985) implemented the finite depth case using the eigenfunction expansion proposed by John (1950), and a Chebyshev polynomial expansion.

In Delhommeau (1989), the algorithm proposed uses an exponential series approximation introduced by Daubisse (1981).

Recently, Liu et al. (2015) presented a modification of Newman's algorithm in which the computational domain is divided into four sub-domains, in which different series expansion schemes are used. When the ratio R/h is small, the author employs Wynn's epsilon algorithm (Wynn 1956) and, when R/h is close to 0, an expansion proposed by Pidcock (1985) is used. The method seems to be as accurate as Newman's method (6 DA), but faster.

A different approach was suggested by Chen (1993), and more recently in Chen (2018). The Rankine part of the Green function is modified, considering five images of the Rankine source instead of one, using the free-surface mirror and the water-bed mirror in relation to the image method, which modifies and simplifies the complexity of the Green function, approximated by smooth and rapidly decay functions. The approximation is different to earlier investigations, concerning the modifications of John's series (90), since direct integration is used. Chen's method (Chen 2018) showed good results, but the derivative of the Green function is still highly oscillatory. No comparison between those models is available yet, for the case of finite depth.

5.3.2 Approximation of the transient Green function

For the time-domain case, Newman (1992) proposed an algorithm to compute the transient Green function and its derivative, in both infinite and finite depth, based on a rational polynomial approximation and Chebyshev polynomial expansion. Bratland and Newman (1997) subsequently updated the finite depth algorithm to overcome the difficulties encountered by Newman (1992).

Some years later, Clément (1999b) found that the Green function is the solution of a fourth-order ordinary differential equation for infinite depth problems. The ODE is integrated by a standard fourth order Runge–Kutta (RK4) procedure. Chuang et al. (2007) and, more recently, Li et al. (2015) continued the development based on Clément's ODE using, instead of RK4, a semi-analytical precise integration method, and an analytical method based on Taylor series expansion, respectively.

Bingham (2016) compared those three ODE-based methods to the method developed by Newman, for an infinite depth fluid. He found that Newman's algorithm was more efficient than any of the ODE-based methods. Moreover, all of the ODE-based methods can only handle infinite depth problems.

5.4 Irregularities in the frequency domain

John (1950) showed that irregularities can appear in the results for certain values of frequencies, where the problem possesses no solution or has a non-unique solution due to ill-conditioning of the linear system. This phenomenon can be an issue, in particular for multi-body interaction problems, where the physical resonance can be confusing with the non-physical irregular value. Two different ways to remove such so-called 'irregular frequencies' are used in the literature; the modified Green function (or modified integral) method, and the extended boundary condition method. Both approaches can be found in the comprehensive reviews of Liu and Falzarano (2017b), and Lee and Newman (2005) (Section 2.7).

The modified Green function method consists of adding singular points onto the interior of the surface, leading to an overdetermined system which guarantees a unique solution. This approach is relatively simple to implement and works well for simple geometries. However, special care needs to be given to the positioning of the singularities, for arbitrary shapes. Lee and Sclavounos (1989) improved this method to adapt it well for arbitrary shapes; nonetheless, the results converge more slowly than the extended boundary condition approach (Lee and Newman 2005).

Since irregular frequencies typically correspond to sloshing modes of the interior space, the extended boundary condition applies a fixed lid condition on the interior free-surface condition. The overdetermined linear system is converted into a square matrix, which is easier to handle. More details on the extended boundary condition approach can be found in Zhu (1994), Liu and Falzarano (2017a) and the user manual (WAMIT Version 7-0, 2013).

6 Rankine sources

Bai and Yeung (1974) were the first to discretise the free-surface using Rankine sources for fixed bodies and bodies undergoing prescribed motions in a three-dimensional unbounded domain, and introduced the concept of mixed Rankine and Green function approach. Later, Dawson (1977) introduced the use of Rankine singularities to solve problems

for bodies moving with forward speed, with low Froude-number theory. In addition to the wetted surface of the body, the line of the undisturbed free-surface is discretised and sources are distributed on it, with numerical approximation used to satisfy the free-surface conditions. A variety of authors have continued Dawson's approach for ships with forward-speed: Raven (1988) highlighted some inconsistencies of Dawson (1977) and showed good results for resistance wave computation, (Sclavounos and Nakos 1988; Nakos and Sclavounos 1990; Kring 1994) made good progress in stability analysis for free-surfaces discretised in both time and space, and (Kim et al. 1997) studied Rankine singularities for zero forward speed problems in the time domain, for fixed bodies and bodies undergoing prescribed motion.

No assumptions are made on the free-surface equations when using Rankine sources, which implies that nonlinear waves can be considered. The development of nonlinear models has been possible, thanks to the pioneering work of Longuet-Higgins and Cokelet (1976), who introduced the mixed Eulerian Lagrangian (MEL) method. The MEL permits to compute fully nonlinear free-surface motions in time-domain, by solving Eulerian field equations to obtain fluid velocity, which allows then to follow fluid particles on the free surface in a Lagrangian way. The MEL approach was first applied for the simulation of steep and overturning waves in two dimensions, without bodies. Faltinsen (1977) used the MEL method for floating bodies, followed by Vinje and Brevig (1981), who considered freely moving floating bodies in two dimensions and introduced the mode decomposition method. Ma et al. (2001) were the first to attempt 3D fully nonlinear simulations for freely moving bodies, thanks to an iterative method.

The use of Rankine sources implies that the radiation condition is not satisfied; hence, an additional treatment of the radiation condition needs to be implemented. Lin et al. (1985), Dommermuth and Yue (1987), and later Scragg and Talcott (1991), used the mixed Rankine–Green function method, whereas Kim et al. (1997) implemented a damping beach to satisfy the radiation condition.

From the general equations obtained in Sect. 2, the integral equation for the potential formulation can be written on the wetted surface of the body S_w and the undisturbed free-surface S_f

$$2\pi\phi(M) + \iint_{S_\mathrm{w}\cup S_\mathrm{f}} \phi(P)\frac{\partial G^R}{\partial n}(M,P)\mathrm{d}S - \iint_{S_\mathrm{w}\cup S_\mathrm{f}} \frac{\partial\phi(P)}{\partial n}G^R(M,P)\mathrm{d}S = 0. \tag{110}$$

In the case of the source formulation, the velocity potential is written as

$$\phi(M) = \iint_{S_\mathrm{w}\cup S_\mathrm{f}} \sigma(P)G^R(M,P)\mathrm{d}P, \tag{111}$$

G^R is the Rankine source defined by

$$G^R = \frac{1}{r}. \tag{112}$$

The domain is discretised over the free-surface elevation and the wetted surface of the body. In case of finite depth problems, additional panels are distributed on the bottom surface, and the normal flux is set to zero.

6.1 Linear waves

In this subsection, we treat the linear case, considering linear free-surface conditions and linear body boundary conditions, only first-order terms are considered, for computational simplicity.

6.1.1 In the time domain

The linearized free-surface condition is satisfied by the addition of Rankine sources over the $z = 0$ plane. After discretization, in time and space, Eq. (110) leads to

$$2\pi\phi^{n+1}(M_i) + \iint_{S_\mathrm{w}\cup S_\mathrm{f}} \phi^{n+1}(P)\frac{\partial G^R}{\partial n}(M_i,P)\mathrm{d}S - \iint_{S_\mathrm{w}\cup S_\mathrm{f}} \left(\frac{\partial\phi}{\partial n}\right)^{n+1}(P)G^R(M_i,P)\mathrm{d}S = 0. \tag{113}$$

The following equation is a linear system which relates the velocity potential to its normal derivative at a collocation point M_i over the domain boundaries, at the $(n+1)$th time step. Using a mixed explicit–implicit Euler scheme for the time discretization of time step Δt, the free-surface conditions (at $z = 0$) become

$$\frac{\phi^{n+1}(M_i) - \phi^n(M_i)}{\Delta t} = -g\eta^{n+1}(M_i), \tag{114}$$

and

$$\frac{\eta^{n+1}(M_i) - \eta^n(M_i)}{\Delta t} = \left(\frac{\partial\phi}{\partial z}\right)^n(M_i). \tag{115}$$

The elimination of the term η^{n+1} in Eq. (114), using (115), leads to

$$\frac{\phi^{n+1}(M_i) - \phi^n(M_i)}{\Delta t} = -g\left(\frac{\partial\phi}{\partial z}\right)^n(M_i)\Delta t - g\eta^n(M_i). \tag{116}$$

Determination of ϕ^{n+1} and η^{n+1} on the free surface The potential of the next $(n+1)$th time step can be determined from knowledge of the potential, its derivative, and the free-surface elevation from the previous nth time step, via Eq. (116). η^{n+1} can also be computed from the previous values η^n and $(\partial\phi/\partial z)^n$, using Eq. (115). Then the derivative $(\partial\phi/\partial z)^{n+1}$ follows from Eq. (113).

6.1.2 Conversion to the frequency domain

Studies using Rankine sources in the frequency domain have been led by authors like Bai and Yeung (1974), Sclavounos and Nakos (1988) or Kim (1999). In the frequency domain, the linearized free-surface condition becomes

$$\frac{\partial\phi}{\partial z}(M_i) - \frac{\omega^2}{g}\phi(M_i) = 0. \tag{117}$$

Kim (1999) converts the time-domain solution to the frequency domain thanks to the Fourier transform. If we can write a time-dependent function $f(t)$ as the following expression

$$f(t) = C_0 + \sum_{n=1}^{N} C_n e^{i\omega_n t}, \tag{118}$$

then the Fourier transform is given by

$$\int_{t_2}^{t_1} f(t)\mathrm{e}^{i\omega_m t}\mathrm{d}t = C_0\sum_{n=1}^{N}\mathrm{e}^{i\omega_m t} + \sum_{n=1}^{N} C_n\int_{t_2}^{t_1} e^{i\omega_n t}\mathrm{e}^{i\omega_m t}\mathrm{d}t, \tag{119}$$

where ω_n is a basis frequency of $f(t)$ with a complex amplitude C, and ω_m is a test frequency. Since the equation is valid for arbitrary test frequencies, there is no restriction on the selection of the basis and test frequencies. The substitution of $N+1$ test frequencies, including a steady component, leads to a linear system of equations which determines C_n. The left-hand side can be evaluated by numerical integration. This provides an efficient Fourier transform for the given time record.

6.2 Nonlinear waves

To deal with a nonlinear free-surface, the MEL method defined by Longuet-Higgins and Cokelet (1976) employs the Lagrangian material derivative, which denotes differentiation following a given particle

$$\frac{D}{Dt} = \frac{\partial}{\partial t} + \nabla\phi.\nabla. \tag{120}$$

The kinematic and the dynamic free-surface conditions can then be written, respectively, as

$$\frac{D\Gamma}{Dt} = u = \nabla\phi, \tag{121}$$

$$\frac{D\phi}{Dt} = -gz + \frac{1}{2}\nabla\phi, \tag{122}$$

with $\Gamma(x, y, z)$ the vector position on the free surface.

To the best of the authors' knowledge, all the existing potential flow codes dealing with a nonlinear free surface use the MEL approach (examples can be found in Kashiwagi 2000; Tanizawa and Minami 2001; Koo and Kim 2004; Ma and Yan 2009; Letournel et al. 2018).

6.3 Stability analysis

Discretising (meshing) the free-surface creates numerical errors, and numerical results can also be polluted by the aliasing phenomenon. Nakos and Sclavounos (1990) and Sclavounos and Nakos (1988) first performed a stability analysis of the free-surface grid in the frequency-domain, for a body with forward speed. The stability analysis is carried out by comparing the continuous and discrete dispersion relations. They concluded that, for a rectangular panel of size (h_x, h_y), the wavelength has to be at least twice as long as the panel in the x and y directions, while the terms (u, v) of the wave number space $k(u, v) = \sqrt{u^2 + v^2}$ cannot be greater than $|u| = \pi/h_x$ and $|v| = \pi/h_y$. Moreover, when the panel ratio $\alpha_{xy} = h_x/h_y$ becomes too large, it can lead to instabilities.

For the case of zero-forward speed in the time domain, Kim et al. (1997) studied the stability by comparing the continuous frequency domain and the discrete (in time and space) dispersion relation for a free surface, in the absence of the body. When the panel ratio α_{xy} is around 1, the greatest source of error comes from the temporal discretisation, for a fixed wavelength, with the error increasing with larger time steps. Kim et al. (1997) established, in Eq. 32 of their publication, a criterion for numerical stability.

6.4 Treatment of the radiation condition

Rankine sources do not satisfy the radiation condition at infinite distance, and the domain has, so far, been assumed to be infinite. Numerical discretization of the free surface of an infinite domain is computationally impractical; therefore, a finite domain is considered. However, the fact is that, in a finite domain, outgoing waves can distort the results by their reflection on the walls of the domain. For problems with forward speed, the technique used by Dawson (1977) is based on a numerical differentiation scheme that numerically guarantees the radiation condition. In the case of zero-forward

speed problems, two principal ways are reported in the literature to treat the radiation condition and avoid reflection. The first method, originally introduced by Israeli and Orszag (1981), includes a wave absorbing zone (usually called a damping beach or sponge layer) between the body and the walls, which satisfies the radiation condition, using numerical damping. The second method, termed the 'hybrid method' or 'mixed source formulation' includes the use of the Green function on the edges of the domain, which automatically satisfies the radiation condition by construction (see Sect. 5). Shin et al. (2003) compared the damping beach and the hybrid method. The mixed source formulation works best for zero and low speeds, while the damping beach is used in the case of higher speeds.

6.4.1 Damping beach

In the case of finite domains, it can be convenient to add an artificial damping term in the boundary integral equations to avoid wave reflections. Such an approach was originally studied by Israeli and Orszag (1981), for different types of waves in two dimensions. Baker et al. (1989) and Cointe (1989) applied numerical damping to water waves for the two-dimensional case, the latter considering a nonlinear free-surface elevation. Kim et al. (1997), Shao (2010), and Letournel et al. (2018) employ the same method for the three-dimensional water wave case. However, the appropriate choice of the optimum damping parameter is not clear, and the work of Israeli and Orszag (1981) did not deal with water waves. For this reason, Kim (2003) published studies on the influence of the damping coefficient for linear and nonlinear water waves. The main advantage of this method is its simplicity to set up. However, the size of the damping zone is usually large, which significantly increases the number of unknowns, and therefore, the computation time.

A cylindrical damping beach is considered in the region $[r_0, r_e]$, with $0 \leq r_0 \leq r_e$. The general representation includes two damping terms in the kinematic free-surface conditions

$$\frac{\partial \eta}{\partial t} - \frac{\partial \phi}{\partial z} + \nabla\phi.\nabla\eta = -\mu_1\eta - \mu_2\phi. \tag{123}$$

The coefficients μ_1 and μ_2 are, respectively, Newtonian cooling and viscous damping terms. Baker et al. (1989), and later Kim (2003), showed that the condition for wave propagation, without phase distortion, is

$$\mu_2 = \frac{\mu_1^2}{4}. \tag{124}$$

A similar route is used by other authors Baker et al. (1989), Cointe (1989), Letournel et al. (2018) in applying a damping coefficient ν on the free-surface elevation η, and potential ϕ, in the (linear or nonlinear) free-surface conditions. In the case of linearized free-surface conditions, we have

$$\frac{\partial \eta}{\partial t} = \frac{\partial \phi}{\partial z} - \nu\eta, \tag{125}$$

$$-\frac{1}{g}\frac{\partial \phi}{\partial t} = \eta - \nu\phi, \tag{126}$$

where ν can be interpreted as the Rayleigh viscosity. Israeli and Orszag (1981) studied the effect of variations in the damping coefficient, and observed good results when ν varies quadratically with the radius $R = \sqrt{x^2 + y^2}$, suggesting a form

$$\nu(R) = \alpha_d \omega \left(\frac{R - r_e}{\lambda_w} - \beta_d \right)^2, \tag{127}$$

where λ_w is the wavelength. The following damping coefficient is used by Cointe (1989) and Letournel et al. (2018), with α_d and β_d of order 1. Kim et al. (1997) employ a slightly different approach from the other authors, but with similar results.

In the frequency domain, Eqs. (125) and (126) lead to

$$\frac{\partial \phi}{\partial z} - \frac{1}{g}(\omega^2 + 2i\nu\omega - \nu^2)\phi = 0. \tag{128}$$

The problem on the free surface S_f is then solved by including Eq. (128) in (110).

The choice of the damping strength plays an important role in the computation, as too small a damping requires a larger part of the free-surface to be meshed, increasing the computational cost. On the other hand, if too much damping is suddenly applied, reflections from within the sponge layer can become significant. Hence, the damping strength has to vanish at the beginning of the damping beach and increase smoothly towards the outer edge.

6.4.2 Hybrid method

The hybrid method was originally introduced by Bai and Yeung (1974), for two-dimensional and simple three-dimensional cases in the frequency domain. Later, Lin et al. (1985), Dommermuth and Yue (1987), Drimer and Agnon (1994) and Gören and Calisal (1998) dealt with the case of nonlinear flows for heaving axisymmetric bodies in the time-domain. Some authors have integrated the hybrid method into their potential flow code (as in, for example, Shin et al. 2003; Liu and Papanikolaou 2011; Li et al. 2017). The idea is to introduce an imaginary cylindrical control surface S_0 around the body. The domain is then divided in an inner domain **I**, where simple Rankine sources are distributed on $S_\mathbf{I}$, and an outer domain **II**, where singularities (which use

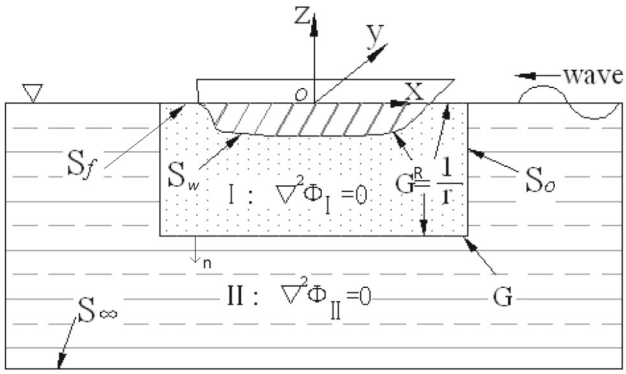

Fig. 3 Inner and outer domains, original figure taken from Liu and Papanikolaou (2011)

the Green function G, and hence linear free-surface conditions) are distributed on $S_{\mathbf{II}}$ (see Fig. 3). The hybrid method uses the advantages of the Rankine sources in the near field, while taking advantage of the Green function in the far field. Lin shows, for the hybrid method in (Lin et al. 1999), good agreement with experimental data, compared to the exclusive use of the Green function, which presents some instability for flared bodies, as highlighted by Wenvang and Yishan (1999).

The use of Rankine sources for potential flow problems does not require any special assumptions, and linear as well as nonlinear free-surface conditions can be considered. Since the outer domain uses linear free-surface conditions, special care should be taken when dealing with nonlinear waves. In three-dimensions, the energy density of a radiated wave decreases inversely with the radial distance. One can then assume that, at a sufficient distance from the body, the radiated wave is sufficiently attenuated to match with the linear boundary conditions of the outer domain (see Lin et al. 1985). In principle, for waves with small steepness, the edges of the control surface S_0 can be located anywhere around the body. This method, though more complex to implement than a damping beach, has the advantage of reducing the number of unknowns on the free surface. Moreover, if the underwater part of the matching surface is constant during time stepping, the time-consuming convolution term of the transient Green function does not have to be re-evaluated (see Lin et al. (1999)).

The inner domain **I** is closed by the wetted surface of the body S_w, the free surface S_f, and the control surface S_0. On these surfaces, the integral equation takes the form of

$$2\pi\phi_{\mathbf{I}}(M) + \iint_{S_\mathrm{w}\cup S_\mathrm{f}\cup S_0} \phi_{\mathbf{I}}(P)\frac{\partial G^R}{\partial n}(M,P)\mathrm{d}S - \iint_{S_\mathrm{w}\cup S_\mathrm{f}\cup S_0} \frac{\partial\phi_{\mathbf{I}}}{\partial n}(P)G^R(M,P)\mathrm{d}S = 0. \tag{129}$$

In the outer domain **II**, the integral equation on the surface S_0 is expressed as

$$2\pi\phi_{\mathbf{II}}(M) + \iint_{S_0} \phi_{\mathbf{II}}(P)\frac{\partial G}{\partial n}(M,P)\mathrm{d}S - \iint_{S_0} \frac{\partial\phi_{\mathbf{II}}}{\partial n}(P)G(M,P)\mathrm{d}S = 0. \tag{130}$$

On the matching surface S_0, the potential and its normal derivative are continuous leading to the matching conditions

$$\begin{cases} \phi_{\mathbf{I}} = \phi_{\mathbf{II}}, \quad \text{on } S_0 \\ \frac{\partial\phi_{\mathbf{I}}}{\partial n} = \frac{\partial\phi_{\mathbf{II}}}{\partial n}. \end{cases} \tag{131}$$

In the time domain, the transient Green function G is given by

$$G = G^0 + G^f, \tag{132}$$

where G^0 is the Rankine source and its image source in the case of infinite depth (105)

$$G^0 = \frac{1}{r} - \frac{1}{r_1}, \tag{133}$$

and G^0 is the Rankine source, its image source and the time-invariant integral in the case of finite depth (109)

$$G^0 = \frac{1}{r} + \frac{1}{r_2} - 2\int_0^\infty \mathrm{e}^{-kh}\frac{\cosh[k(c+h)]\cosh[k(z+h)]}{\cosh kh}J_0(kR)\mathrm{d}k, \tag{134}$$

and G^f is the time-dependent memory part of the Green function of (105) and (109), for infinite and finite depth, respectively. Therefore, the integral equation of the outer domain (130) can be re-written (Lin et al. 1999) as follows:

$$\begin{aligned} 2\pi\phi_{\mathbf{II}}(M) &+ \iint_{S_0}\left(\phi_{\mathbf{II}}(P)\frac{\partial G^0}{\partial n}(M,P)\mathrm{d}S - \frac{\partial\phi_{\mathbf{II}}}{\partial n}(P)G^0(M,P)\right)\mathrm{d}S \\ &= \int_0^t \mathrm{d}\tau \iint_{S_0}\left(\phi_{\mathbf{II}}(P)\frac{\partial G^f}{\partial n}(M,P)\mathrm{d}S - \frac{\partial\phi_{\mathbf{II}}}{\partial n}(P)G^f(M,P)\right)\mathrm{d}S. \end{aligned} \tag{135}$$

The matching conditions (131), along with the integral equations for $\phi_{\mathbf{I}}$, (129), $\phi_{\mathbf{II}}$ (135) and their normal derivatives, form a coupled equation system for the potential $\phi_{\mathbf{I}}$ on S_w, $\partial\phi_{\mathbf{I}}/\partial n$ on S_f, and $\phi_{\mathbf{I}}$ and $\partial\phi_{\mathbf{I}}/\partial n$ on S_0.

The approach to time discretization is the same as that developed in Sect. 6.1.1; at a given time step, the potential $\phi_{\mathbf{I}}$ on S_{f} is known, so is its normal derivative on S_{w}. Using the free-surface conditions, one can, therefore, compute the free-surface elevation, and the problem can then be solved on S_{w}, S_{f} and S_0.

In the frequency-domain case (see Bai and Yeung 1974), the Green functions obtained in (78) and (87) are used to compute the potential in the outer domain for infinite and finite depth, respectively. They satisfy, by construction, the Sommerfeld radiation condition mentioned in (58).

7 Hydrodynamic loads and equations of motion

When dealing with moving bodies, it is necessary to compute the hydrodynamic forces which are acting on the body surface. Newton's second law leads to the equation of motion, linking the acceleration of the body to the hydrodynamic forces (11). However, hydrodynamic forces depend on the time derivative of the potential (9), and the time derivative of the potential itself depends on the body acceleration through the body boundary condition (6), which makes the problem strongly coupled between the body motion and the potential.

In the case of fixed bodies, or bodies undergoing prescribed motion, the acceleration is already known and the problem can be solved, but in the case of freely moving bodies the acceleration is not known a priori. Different methods have been implemented to deal with this strong coupling, and are separated into two families of methods: the approaches more suitable for the Green function, and the methods more appropriated for Rankine sources. Technically, the methods more suitable for Green function could be chosen using Rankine singularities (and vice versa), but, to the best of the authors' knowledge, no studies have considered those cases.

7.1 Hydrodynamic forces using the Green function formulation

The hypothesis of small wave steepness and small body motion enable to consider linearity in the equations. When we consider a body undergoing prescribed or free motion with or without regular waves, or fixed bodies in presence of regular incident waves, a frequency-domain approach can be used. In the case of a moving body (freely or undergoing prescribed motion) or fixed bodies submitted to irregular incident waves, a time-domain approach is considered.

7.1.1 Frequency-domain formulation

If we consider waves of an angular frequency ω, we can then extend the complex notation originally introduced in (44) by considering the total complex velocity potential φ

$$\phi = \Re(\varphi e^{-i\omega t}). \tag{136}$$

The decomposition of the total velocity potential expressed in (20) can then be applied in the frequency domain as follows:

$$\varphi = \varphi_0 + \varphi_D + \varphi_R, \tag{137}$$

with φ_0, φ_D and φ_R the complex incident, diffraction and radiation velocity potential, respectively. The complex incident velocity potential can be retrieved from (57) and is given by

$$\varphi_0 = -\frac{a_{\mathrm{w}} g}{\omega} \frac{\cosh(k_0(z+h))}{\cosh(k_0 h)} e^{ik_0 x}, \tag{138}$$

with a_{w} the wave amplitude, h the water depth, $k_0 = 2\pi/\lambda_w$ the wave number, $\omega = 2\pi/T_{\mathrm{w}}$ the angular frequency, where λ_{w} and T_{w} are the wavelength and wave period, respectively. The complex generalized hydrodynamic forces are expressed as

$$F_i = \iint_{S_{\mathrm{w}}} \Re(i\rho\omega\varphi_i e^{-i\omega t}) n_{0i} \mathrm{d}s = \Re(\mathbf{F}_i \mathrm{e}^{-i\omega t}), \tag{139}$$

with

$$\mathbf{F}_i = i\rho\omega \iint_{S_{\mathrm{w}}} (\varphi_0 + \varphi_D) n_i \mathrm{d}s + \sum_{j=1}^{6} i\rho\omega V_j \iint_{S_{\mathrm{w}}} \varphi_{Rj} n_i \mathrm{d}s. \tag{140}$$

We can then separate the terms on the right-hand side of (140) into excitation forces $\mathbf{F}_i^{\mathrm{ex}}$ and radiation forces $\mathbf{F}_i^R$ as

$$\mathbf{F}_i = \mathbf{F}_i^{\mathrm{ex}} + \mathbf{F}_i^R, \tag{141}$$

where $\mathbf{F}_i^{\mathrm{ex}}$ are the forces exerted on the stationary body, and $\mathbf{F}_i^R$ corresponds to the forces exerted on the body in motion, without incident waves present.

Excitation forces The excitation forces are divided into Froude–Krylov forces $\mathbf{F}_i^{\mathrm{FK}}$, which are the forces exerted by the pressure of the incident wave, and diffraction forces $\mathbf{F}_i^D$

$$\mathbf{F}_i^{\mathrm{ex}} = \mathbf{F}_i^{\mathrm{FK}} + \mathbf{F}_i^D = i\rho\omega \iint_{S_{\mathrm{w}}} \varphi_0 n_i \mathrm{d}s + i\rho\omega \iint_{S_{\mathrm{w}}} \varphi_D n_i \mathrm{d}s, \tag{142}$$

which gives

$$F_{\mathrm{ex}\,i}(t) = \Im\left((\mathbf{F}_i^{\mathrm{FK}} + \mathbf{F}_i^D)\mathrm{e}^{-i\omega t}\right). \tag{143}$$

Radiation forces The radiation forces $\mathbf{F}_i^R$ can be written as

$$\mathbf{F}_i^R = \sum_{j=1}^{6} i\rho\omega V_j \iint_{S_w} \varphi_{Rj} n_i \mathrm{d}s = \sum_{j=1}^{6} \mathbf{f}_{ij} V_j, \tag{144}$$

where $\mathbf{f}_{ij}$ is the load exerted in direction i, due to a unit velocity motion in the jth degree of freedom. The total radiation load can be detailed as

$$F_{Ri}(t) = \Re(\mathbf{f}_{ij} V_j e^{-i\omega t}) = \Re[(\Re\mathbf{f}_{ij} + \Im\mathbf{f}_{ij}) V_j \mathrm{e}^{-i\omega t}], \tag{145}$$

or

$$F_{Ri}(t) = \Re\left(\left[\rho\omega \iint_{S_w} \Im(\varphi_{Rj}) n_i \mathrm{d}s + i\rho\omega \iint_{S_w} \Re(\varphi_{Rj}) n_i ds\right][V_j \mathrm{e}^{-i\omega t}]\right). \tag{146}$$

Then writing the body velocity $\dot{X}$, and its acceleration $\ddot{X}$, as

$$\dot{X} = V, \tag{147}$$
$$\ddot{X} = -i\omega V, \tag{148}$$

we obtain

$$F_{Ri}(t) = -\left(\rho \iint_{S_w} \Re(\varphi_{Rj}) n_i \mathrm{d}s\right) \ddot{X}_j - \left(\rho\omega \iint_{S_w} \Im(\varphi_{Rj}) n_i \mathrm{d}s\right) \dot{X}_j. \tag{149}$$

The radiation forces are composed of a term proportional to the body acceleration, with a further term proportional to the body velocity. The first term behaves like an added mass. This part of the radiation forces is thus formalized using the added mass term

$$\mu_{ij} = \rho \iint_{S_w} \Re(\varphi_{Rj}) n_i \mathrm{d}s = \frac{1}{\omega} \Im(\mathbf{f}_{ij}). \tag{150}$$

The second term is a damping term, expressed as

$$\lambda_{ij} = \rho\omega \iint_{S_w} \Im(\varphi_{Rj}) n_i \mathrm{d}s = -\Re(\mathbf{f}_{ij}). \tag{151}$$

According to these definitions, the radiation forces can now be written as

$$F_{Ri}(t) = -\sum_{j=1}^{6} \mu_{ij} \ddot{X}_j(t) - \sum_{j=1}^{6} \lambda_{ij} \dot{X}_j(t). \tag{152}$$

Equation of motion The linearized equation of motion derived from (11) can be expressed in the frequency domain, obtaining the following linear hydrodynamic formulation:

$$\mathbf{M}_{ji} \ddot{X}_i(t) = \left(F_{Hj} + F_{exj} + F_{Rj}\right) \mathrm{e}^{-i\omega t}, \tag{153}$$

with $\mathbf{M}$ the mass matrix. Equation (153) can be developed as follows:

$$(\mathbf{M}_{ji} + \mu_{ji}) \ddot{X}_i(t) + \lambda_{ji} \dot{X}_i(t) + K_{Hji} X_i(t) = \mathbf{F}_j^{ex} \mathrm{e}^{-i\omega t}, \tag{154}$$

or, if we write $X(t) = \Re(\mathbf{X}\mathrm{e}^{-i\omega t})$

$$[-\omega^2(\mathbf{M}_{ji} + \mu_{ji}) - i\omega\lambda_{ji} + K_{Hji}]\mathbf{X}_i = \mathbf{F}_j^{\mathrm{ex}}. \tag{155}$$

7.1.2 Time-domain formulation

The time-domain problem is solved using the impulse response function in different, but somewhat similar ways, for the radiation and the diffraction problems. We assume the impulse happening at $t = \tau$ and the potential to be at rest at $t < \tau$.

Radiation problem Cummins (1962) proposed a new decomposition of the potential based on the impulse response function. If we consider an impulse velocity imposed on a body, in one of its degree of freedom i, we can write

$$\dot{X}_i(t) = \delta(t), \tag{156}$$

where $\delta(t)$ is the Dirac delta function. We consider the following decomposition of the impulse potential $\phi_{Ri}^{\Delta}(t)$

$$\phi_{Ri}^{\Delta}(t) = \delta(t)\phi_{Ri}^{\delta} + H(t)\phi_{Ri}^{H}(t), \tag{157}$$

where H is the Heaviside function. Assuming that we can find a solution satisfying the Laplace equation (2), the sea-bottom (5) and radiation conditions, and the linearized free-surface (23) and body (24) boundary conditions, we can build the response to an arbitrary velocity potential by convolution with the impulse potential, exploiting the linearity of the problem

$$\phi_R(t) = \sum_{i=1}^{6} \int_{-\infty}^{\infty} \dot{X}_i(t) \phi_{Ri}^{\Delta}(t-\tau) \mathrm{d}\tau, = \sum_{i=1}^{6} \left(\dot{X}_i(t)\phi_{Ri}^{\delta} + \int_{-\infty}^{\infty} H(t-\tau)\dot{X}_i(t)\phi_{Ri}^{H}(t-\tau)\mathrm{d}\tau\right). \tag{158}$$

Equation (158) can then be written as

$$\phi_R(t) = \sum_{i=1}^{6} \left(\dot{X}_i(t)\phi_{Ri}^{\delta} + \int_0^{\infty} \dot{X}_i(t-\tau)\phi_{Ri}^{H}(\tau)\mathrm{d}\tau \right), \tag{159}$$

or

$$\phi_R(t) = \sum_{i=1}^{6} \left(\dot{X}_i(t)\phi_{Ri}^{\delta} + \int_{-\infty}^{t} \dot{X}_i(\tau)\phi_{Ri}^{H}(t-\tau)\mathrm{d}\tau \right). \tag{160}$$

Using Eq. (157), the body boundary conditions (24) can be re-written as

$$\frac{\partial \phi_{Ri}^{\Delta}}{\partial n}(t) = \delta(t).n_i, \quad \text{on } S_{\mathrm{w}}, \tag{161}$$

which implies

$$\frac{\partial \phi_{Ri}^{\delta}}{\partial n} = n_i, \quad \frac{\partial \phi_{Ri}^{H}}{\partial n}(t) = 0, \quad \text{on } S_{\mathrm{w}}. \tag{162}$$

By developing the terms included in the linearized free-surface condition (23), we have

$$\frac{\partial \phi_{Ri}^{\Delta}}{\partial t} = \dot{\delta}(t)\phi_{Ri}^{\delta} + H(t)\dot{\phi}_{Ri}^{H}(t) + \delta(t)\phi_{Ri}^{H}(t), \tag{163}$$

$$\frac{\partial^2 \phi_{Ri}^{\Delta}}{\partial t^2} = \ddot{\delta}(t)\phi_{Ri}^{\delta} + H(t)\ddot{\phi}_{Ri}^{H}(t) + 2\delta(t)\dot{\phi}_{Ri}^{H}(t) + \dot{\delta}(t)\phi_{Ri}^{H}(t=0), \tag{164}$$

and

$$g\frac{\partial \phi_{Ri}^{\Delta}}{\partial z} = g\left[\delta(t)\frac{\partial \phi_{Ri}^{\delta}}{\partial z} + H(t)\frac{\partial \phi_{Ri}^{H}}{\partial z}(t) \right]. \tag{165}$$

The free-surface condition becomes

$$H(t)\left[\frac{\partial^2 \phi_{Ri}^{H}}{\partial t^2}(t) + g\frac{\partial \phi_{Ri}^{H}}{\partial z}(t) \right] + \delta\left[2\delta(t)\dot{\phi}_{Ri}^{H}(t) + g\frac{\partial \phi_{Ri}^{\delta}}{\partial z} \right] + \dot{\delta}(t)\phi_{Ri}^{H}(t=0) + \ddot{\delta}(t)\phi_{Ri}^{\delta} = 0, \quad \text{on } z = 0. \tag{166}$$

Hence, new conditions appear as

$$\phi_{Ri}^{\delta} = 0, \quad \frac{\partial^2 \phi_{Ri}^{H}}{\partial t^2} + g\frac{\partial \phi_{Ri}^{H}}{\partial z} = 0, \quad \text{on } z = 0, t > 0, \tag{167}$$

and

$$\phi_{Ri}^{H} = 0, \quad 2\frac{\partial \phi_{Ri}^{H}}{\partial t} + g\frac{\partial \phi_{Ri}^{\delta}}{\partial z}, \quad \text{on } z = 0, t = 0. \tag{168}$$

To obtain the radiation forces, the pressure on the body needs to be known (40), which implies to compute the time derivative of the potential (38). The time derivative of (160) is given by

$$\frac{\partial \phi_R}{\partial t}(M,t) = \sum_{i=1}^{6} \left(\ddot{X}_i(t)\phi_{Ri}^{\delta}(M) + \int_{-\infty}^{t} \ddot{X}_i(\tau)\phi_{Ri}^{H}(M, t-\tau)\mathrm{d}\tau \right), \tag{169}$$

which gives the radiation force as

$$F_{Rj} = \sum_{i=1}^{6} \left(-\ddot{X}_i(t)\left[\rho \int_{S_{\mathrm{w}}} \phi_{Ri}^{\delta}(M) n_j \mathrm{d}S \right] - \int_{-\infty}^{t} \int_{S_{\mathrm{w}}} \rho \ddot{X}_i(\tau)\phi_{Ri}^{H}(M, t-\tau) n_j \mathrm{d}S \mathrm{d}\tau \right). \tag{170}$$

If we write the added mass at infinite frequency $\mu(\infty)$ and the radiation kernel $L(t)$ as follows:

$$\mu_{ji}(\infty) = \rho \int_{S_{\mathrm{w}}} \phi_{Ri}^{\delta}(M) n_j \mathrm{d}S, \tag{171}$$

$$L_{ji}(t) = \rho \int_{S_{\mathrm{w}}} \phi_{Ri}^{H}(M, t-\tau) n_j \mathrm{d}S, \tag{172}$$

with $i, j = 1 \ldots 6$ we then have the radiation forces

$$F_{Rj} = \sum_{i=1}^{6} \left(-\ddot{X}_i(t)\mu_{ji}(\infty) - \int_{-\infty}^{t} \ddot{X}_i(\tau) L_{ji}(t-\tau)\mathrm{d}\tau \right). \tag{173}$$

It can be shown, with the linearized free-surface condition in frequency domain

$$-\omega^2 \phi_{Ri} + g\frac{\partial \phi_{Ri}}{\partial z} = 0, \quad \text{on } z = 0, \tag{174}$$

that when $\omega \to +\infty$, Eq. (174) becomes $\phi_{Ri}(z=0) = 0$, and

$$\lim_{\omega \to +\infty} \phi_{Ri} = \phi_{Ri}^{\delta}, \quad \lim_{\omega \to +\infty} \mu_{ji} = \mu_{ji}(\infty). \tag{175}$$

Diffraction problem In the diffraction problem, the body is assumed fixed and impinged upon by an impulse incident wave elevation $\eta_0^{\Delta}(t)$ at $t = \tau$

$$\eta_0^{\Delta}(t) = \delta(t). \tag{176}$$

The resulting impulse diffraction potential ϕ_D^Δ satisfies the Laplace equation (2), the sea-bottom (5) and radiation conditions, and the linearized free-surface (23) and body (24) boundary condition. The body boundary condition is given by

$$\frac{\partial \phi_D^\Delta}{\partial n} = -\frac{\partial \phi_0^\Delta}{\partial n}, \quad \text{on } S_\text{w}, \tag{177}$$

ϕ_0^Δ being the impulse incident potential. Assuming that the problem has a solution, we can build the response to an arbitrary wave by convolution with the impulse diffraction potential,

$$\phi_D(t) = \int_{-\infty}^{+\infty} \eta_j(t-\tau)\phi_D^\Delta(\tau)\mathrm{d}\tau, \tag{178}$$

or

$$\phi_D(t) = \int_{-\infty}^{+\infty} \eta_j(\tau)\phi_D^\Delta(t-\tau)\mathrm{d}\tau. \tag{179}$$

We then have the diffraction forces

$$F_{Dj}(t) = -\rho \int_{-\infty}^{+\infty} \int_{S_\text{w}} \eta_j(\tau)\frac{\partial \phi_D^\Delta}{\partial t}(t-\tau)\mathrm{d}S\mathrm{d}\tau, \tag{180}$$

and the Froude–Krylov forces

$$F_{\text{FK}j}(t) = -\rho \int_{-\infty}^{+\infty} \int_{S_\text{w}} \eta_j(\tau)\frac{\partial \phi_0^\Delta}{\partial t}(t-\tau)\mathrm{d}S\mathrm{d}\tau. \tag{181}$$

Equation of motion The linearized equation of motion derived from (11) can be expressed in the time domain

$$\begin{aligned}&(\mathbf{M}_{ji} + \mu_{ji}(\infty))\ddot{X}_i(t) + L_{ji}(t) * \dot{X}_i(t)\\ &+K_{Hji}X_i(t) = F_{exj}(t),\end{aligned} \tag{182}$$

where $L_{ji}(t) * \dot{X}_i(t)$ represents the convolution product between $L(t)$ and body velocity $\dot{X}(t)$.

7.1.3 Time–frequency equivalence

Ogilvie (1966) established a direct relationship between the time-domain and frequency-domain models, as a function of the added-mass $\mu_{ji}(\omega)$, radiation damping $\lambda_{ji}(\omega)$, and the radiation kernel $L_{ji}(t)$, using the definition of the Fourier transform. If we assume time periodicity

$$V_i = \Re(\mathbf{V}_i e^{-i\omega t}), \tag{183}$$

and that the motion has lasted for $t \to +\infty$, Eq. (159) can be written

$$\begin{aligned}\phi_R(t) &= \sum_{i=1}^{6} \Re(\mathbf{V}_i \mathrm{e}^{-i\omega t})\phi_{Ri}^\delta + \int_0^\infty \Re(\mathbf{V}_i \mathrm{e}^{-i\omega(t-\tau)})\phi_{Ri}^H(\tau)\mathrm{d}\tau,\\ &= \sum_{i=1}^{6} \Re\left(\left[\phi_{Ri}^\delta + \int_0^\infty \phi_{Ri}^H(\tau)\mathrm{e}^{i\omega(\tau)}\mathrm{d}\tau\right]\mathbf{V}_i \mathrm{e}^{-i\omega t}\right).\end{aligned} \tag{184}$$

Equation (136) then gives

$$\varphi_{Ri}(M,\omega) = \phi_{Ri}^\delta + \int_0^\infty \phi_{Ri}^H(\tau)\mathrm{e}^{i\omega(\tau)}\mathrm{d}\tau. \tag{185}$$

Hence, the radiation forces are given by

$$\begin{aligned}F_{Rj}(t) &= \Re\left(\sum_{i=1}^{6}\left[\rho\int_{S_\text{w}} \phi_{Ri}^\delta n_j \mathrm{d}S\right.\right.\\ &\left.\left.+\rho\int_0^\infty e^{i\omega(\tau)}\mathrm{d}\tau\int_{S_\text{w}}\phi_{Ri}^H(\tau)n_j\mathrm{d}S\right]i\omega\mathbf{V}_i\mathrm{e}^{-i\omega t}\right),\\ &= \Re\left(\sum_{i=1}^{6}\left[\mu_{ji}(\infty) + \int_0^\infty L_{ji}(\tau)\mathrm{e}^{i\omega(\tau)}\mathrm{d}\tau\right]i\omega\mathbf{V}_i e^{-i\omega t}\right).\end{aligned} \tag{186}$$

The definition of the radiation forces in the frequency domain, given in Eq. (152), can now be written

$$F_{Rj}(t) = \Re\left(\sum_{i=1}^{6}\left[\mu_{ji}(\omega) + i\frac{\lambda_{ji}}{\omega}(\omega)\right]i\omega\mathbf{V}_i\mathrm{e}^{-i\omega t}\right). \tag{187}$$

Hence, we have, by equivalence, we obtain the following relation:

$$\mu_{ji}(\omega) + i\frac{\lambda_{ji}}{\omega}(\omega) = \mu_{ji}(\infty) + \int_0^\infty L_{ji}(\tau)\mathrm{e}^{i\omega(\tau)}\mathrm{d}\tau. \tag{188}$$

By separating the real and imaginary parts, we obtain

$$\mu_{ji}(\omega) - \mu_{ji}(\infty) = \int_0^\infty L_{ji}(\tau)\cos(\omega\tau)\mathrm{d}\tau, \tag{189}$$

$$\lambda_{ji}(\omega) = \omega\int_0^\infty L_{ji}(\tau)\sin(\omega\tau)\mathrm{d}\tau. \tag{190}$$

It follows that the impulse response $L_{ji}(t)$ can be written as a mapping involving the frequency-dependent parameters as

$$L_{ji}(t) = \frac{2}{\pi}\int_0^{+\infty}\frac{\lambda_{ji}(\omega)}{\omega}\sin(\omega t)\mathrm{d}\omega. \tag{191}$$

Equation (191) facilitates a frequency-domain analysis of $L(t)$, where a direct application of the Fourier transform yields

$$L_{ji}(j\omega) = [\mu_{ji}(\omega) - \mu_{ji}(\infty)] + i\frac{\lambda_{ji}(\omega)}{\omega}, \tag{192}$$

which, considering the real and imaginary parts, $\Re(L_{ji}(j\omega))$ and $\Im(L_{ji}(j\omega))$, leads to a frequency-domain description for $\mu_{ji}(\omega)$ and $\lambda_{ji}(\omega)$ as

$$\begin{aligned} \lambda(\omega) &= \omega\Im(L_{ji}(j\omega)), \\ \mu_{ji}(\omega) &= \Re(L_{ji})(j\omega) + \mu_{ji}(\infty). \end{aligned} \tag{193}$$

7.2 Hydrodynamic forces using Rankine sources

The methods reviewed in this section to evaluate the hydrodynamic forces do not make any assumption on the wave steepness and the body motion. To compute the hydrodynamic loads, the time derivative of the potential on the wetted surface of the body has to be computed

$$\frac{\partial^2\phi}{\partial n \partial t} = \ddot{X}_T.n + q \quad \text{on } S_\text{w}, \tag{194}$$

with

$$\begin{aligned} q = {} & (\Theta.s_1)\left(\frac{\partial\phi}{\partial s_2} - 2(\dot{X}_T.s_2)\right) \\ & - (\Theta.s_2)\left(\frac{\partial\phi}{\partial s_1} - 2(\dot{X}_T.s_1)\right) \\ & + \frac{(\dot{X}_T.s_1)}{c_1}\left(\frac{\partial\phi}{\partial s_1} - (\dot{X}_T.s_1)\right) \\ & + \frac{(\dot{X}_T.s_2)}{c_2}\left(\frac{\partial\phi}{\partial s_2} - (\dot{X}_T.s_2)\right) \\ & + (\dot{X}_T.n)\left(\frac{\partial^2\phi}{\partial s_1^2} + \frac{\partial^2\phi}{\partial s_2^2} + \left(\frac{1}{c_1} + \frac{1}{c_2}\right)\frac{\partial\phi}{\partial n}\right), \end{aligned} \tag{195}$$

where $\ddot{X}_T$ is the acceleration vector of the body in translation, and q corresponds to the the advection term, due to the body motion. Θ represents the body rotational vector according to the Euler angles $\dot{\psi_E}$, $\dot{\theta_E}$, and $\dot{\varphi_E}$ (see Fig. 4)

$$\Theta = \dot{\psi_E} + \dot{\theta_E} + \dot{\varphi_E}, \tag{196}$$

s_1 and s_2 are the local coordinates vectors, and c_1 and c_2 are the local curvature along the respective local vectors. More details on the method to compute the time derivative of the potential are given in Letournel et al. (2017) and Letournel et al. (2018).

The time derivative of the potential is not known and can be determined in two different ways. When the body is fixed or undergoing prescribed motion, it is not necessary to compute hydrodynamic loads. The potential on the body is known at each time step, and a finite difference scheme can be used, as a post-processing step, to estimate its time derivative, which leads to the hydrodynamic loads.

In the case of a body undergoing free motion, the finite difference method is not appropriate for computation of the time derivative of the potential and can lead to instabilities (an example can be found in Cointe 1991), due to strong coupling between the body motion dynamics and the hydrodynamic loads. The potential and the body acceleration must be computed by solving a coupled fluid–structure interaction problem, in which equations for the fluid and body motion are simultaneously solved. Four methods have been developed in the literature (reviewed in Koo and Kim 2004) to compute the time derivative of the potential for freely floating bodies: the mode decomposition, the indirect method, the iterative method and the implicit methods.

7.2.1 The mode decomposition

Originally proposed by Vinje and Brevig (1981), and used by Koo and Kim (2004) and Cointe (1991), the mode decomposition was the first method introduced to compute fully nonlinear problems with floating bodies. The mode decomposition consists in a linear decomposition of the time derivative of the potential, into six modes corresponding to the unit accelerations for the six degrees of freedom (three modes for 2D problems), and one mode corresponding to the acceleration due to the velocity field (see Koo and Kim 2004 for further details). Each mode is obtained by solving the respective boundary integral equation. The seven modes are computed at each iteration and lead to a value of the time derivative of the potential $\partial\phi/\partial t$. The body displacement is then calculated with the equation of motion (11), and yields to the body acceleration, which permits to the body displacement and velocity to be time integrated for the next time step. The main drawback of the mode decomposition, originally developed for 2D problems, is that the method is very time-consuming, as seven boundary value problems (BVP) have to be solved to compute $\partial\phi/\partial t$, which considerably increases the computation time.

7.2.2 The indirect method

The indirect method, suggested by Wu and Taylor (1996), and followed by other authors like Bai and Taylor (2009), Wang et al. (2007), is based on the fact that it is not necessary to compute explicitly the time derivative of the potential $\partial\phi/\partial t$ to access the body acceleration. Indeed, the term $\partial\phi/\partial t$ needs to be computed only if the hydrodynamic forces (9) exerted on the body are of interest. Six auxiliary functions are introduced, one for each degree of freedom, where each of them

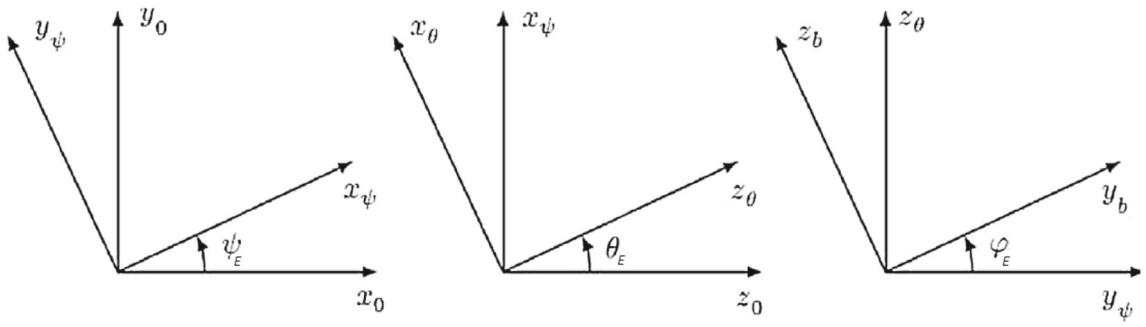

Fig. 4 Euler angles $\dot{\psi_E}, \dot{\theta_E}, \dot{\varphi_E}$ with their corresponding vector. (x_b, y_b, z_b) is the right-handed coordinate system linked to the body

is a solution of the Laplace equation with specific boundary conditions. The forces are then expressed as a function of coefficients, that depend on these auxiliary functions. By use of Green's second identity the coefficients can be linked to the acceleration of the body. The equation of motion is then solved by substituting in the latter relation the obtained potential and the auxiliary functions. In case that the hydrodynamic forces are required, an additional BVP for $\partial\phi/\partial t$ has to be solved. The mode-decomposition method and the indirect method are mathematically identical, and only vary by an integral term that can be replaced by other equivalent terms in the indirect method.

7.2.3 The iterative method

Proposed by Cao et al. (1994) and used by Sen (1993) or Ma and Yan (2009), the iterative method lies in the estimation of the body acceleration at the current time step, based on the values of the body acceleration at the previous time steps. The prediction of the acceleration is made by curve fitting, and the velocity is then estimated thanks to an Adam–Basforth implicit scheme. Using equation (194), $\partial\phi/\partial t$ can then be computed as a solution of a Laplace equation with explicit boundary conditions, leading to the hydrodynamic forces. The body acceleration is computed through the equation of motion (11), and a correction is applied on the forces or the acceleration, which are compared to their initially estimated values. The method is repeated until convergence is reached. The body displacement and velocity are then time integrated to the next time step.

In the iterative method developed by Cao et al. (1994), as well as the mode decomposition or the indirect method, the body velocity is estimated from the acceleration at previous time steps, which makes the time marching procedure explicit, which may degrade the accuracy and can lead to instabilities, unless sufficient small time steps are used, which makes the computation time-consuming. An extension of the iterative method, called iterative semi-implicit time integration method for floating bodies procedure (ISITIMFB-M), has been suggested by Ma and Yan (2009), where the body velocity is computed implicitly, which allows to consider bigger time steps. The iterative method may be time-consuming if convergence is not quickly reached.

7.2.4 The implicit method

The implicit method has been introduced by van Daalen (1993), and Tanizawa (1995) under the name 'acceleration potential method', and recently used by Guerber (2011) and Letournel et al. (2018). The principle lies in the fact that the time derivative of the body boundary condition links the acceleration of the body and the normal derivative of the potential $\partial\phi/\partial n$ to its time derivative $\partial^2\phi/\partial t\partial n$. Then the equation of motion is substituted to the time derivative of the body boundary condition, allowing to remove the acceleration of the body. An extra boundary value problem (BVP) for the time derivative of the potential is added (including the time derivative of the body boundary condition). It is, therefore, possible to solve implicitly the velocity potential and its time derivative before an explicit calculation of the acceleration of the body (see Letournel et al. 2018 for further details). The implicit method seems less time-consuming than the other methods, since only two BVP need to be solved at each time step to access the hydrodynamic forces and the acceleration of the body. The BVP on the time derivative of the potential is similar to the one for the potential, and is given by

$$\Delta\phi = 0 \Rightarrow \Delta\frac{\partial\phi}{\partial t} = 0, \tag{197}$$

$$\begin{cases} \Delta\frac{\partial\phi}{\partial t} = 0 \quad \text{in the fluid domain } D, \\ \frac{\partial\phi}{\partial t} = \frac{D_{0_Z}\phi}{Dt} - \frac{\partial\phi_0}{\partial z}\frac{\partial\phi}{\partial z} \quad \text{on } S_f, \\ \frac{\partial^2\phi}{\partial n\partial t} = \ddot{X}_T.n + q \quad \text{on } S_w, \\ \frac{\partial^2\phi}{\partial n\partial t} = 0 \quad \text{on the boundaries.} \end{cases} \tag{198}$$

8 Nonlinear potential flow models

Linear potential flow theory has been largely used in free-surface potential flow problems. Results based on this theory have shown, in general, good agreement with experiments for wave–structure interaction problems like wave resistance, hydrodynamic forces or body motion calculations. However, the fully linear approach has its limitations, in particular for wave energy converters (WEC), where the assumptions of small motion cannot be made, especially when control is applied to maximize power absorption (and amplify the WEC motion), as well as with severe sea states, where waves with small steepness can no longer be considered. Moreover, when dealing with long and thin-shaped bodies (like ships), assumptions of small radiation or diffraction forces are reasonable, which might not be the case for bodies of arbitrary shapes. Some physical phenomena, such as parametric roll shown by Babarit et al. (2009) also cannot be predicted by the linear potential flow theory.

The need of including nonlinearities led to different models with different degrees of assumptions: the linear theory extended to second-order effects, the body-exact, weak-scatterer and fully nonlinear models. The body-exact is a partially nonlinear model which takes into account the body motion with a free-surface linearized around the plane $z = 0$. The weak scatterer is a weakly nonlinear model which goes one step further in taking into account nonlinearities, by dealing with a linearized free surface around the incident wave elevation η_0. The fully nonlinear method does not make any additional assumptions. These models are presented next.

8.1 Extension of linear model to second order

The extension of the linear model to second order was the first model to consider nonlinearities, with comprehensive review presented by Ogilvie (1983). Some phenomena that cannot be predicted by first-order linear theory appear when looking at second-order effects, such as mean drift forces acting on a body. Moreover, a moored body usually has natural frequencies of oscillation far below the frequencies of incident waves which, when considering second-order excitation, leads to resonance of the system at low frequency.

The extension to the second order is obtained by applying a perturbation method on the total potential ϕ and free-surface elevation η as follows:

$$\phi = \epsilon\phi_1 + \epsilon^2\phi_2, \tag{199}$$

$$\eta = \epsilon\eta_1 + \epsilon^2\eta_2, \tag{200}$$

where ϵ is the wave steepness parameter, ϕ_1 and η_1 are, respectively, the potential and free-surface elevation of the first order discussed in Sect. 4, ϕ_2 and η_2 are, respectively, the second-order potential and free-surface elevation. This leads to a second-order boundary value problem (BVP), similar to the first-order problem, with

- the Laplace equation

$$\Delta\phi_2 = 0, \tag{201}$$

- second-order free-surface boundary conditions (on $z = 0$)

$$\eta_2 = -\frac{1}{g}\left(\frac{\partial\phi_2}{\partial t} + \frac{\partial^2\phi_1}{\partial t\partial z}\eta_1 + \frac{1}{2}\nabla\phi_1.\nabla\phi_1\right), \tag{202}$$

$$\frac{\partial^2\phi_2}{\partial t^2} + g\frac{\partial\phi_2}{\partial z} = -2\nabla\phi_1.\nabla\frac{\partial\phi_1}{\partial t} + \frac{\partial\phi_1}{\partial t}\left(\frac{\partial^2\phi_1}{\partial z^2} + \frac{1}{g}\frac{\partial^3\phi_1}{\partial t^2\partial z}\right), \tag{203}$$

- the impermeability condition on the seabed

$$\frac{\partial\phi_2}{\partial n} = 0, \tag{204}$$

- the radiation condition, where the radiation and diffraction second-order potentials tends to 0 moving away from the body, and
- the body boundary condition.

Further details about the body boundary condition and the method to compute the second-order forces can be found in Ogilvie (1983). An example of a floating axisymmetric body, in 2D, using the second-order formulation, is given in Drimer and Agnon (1994). Faltinsen (1975) and Pinkster and Van Oortmerssen (1978) computed a 3D numerical solution for barge-like bodies, including the drift force; some years later Papanikolaou (1985) extended the method for arbitrarily shaped floating bodies. Regarding axisymmetric bodies, Molin (1979) solved the second-order diffraction problem for fixed bodies in 3D, and Gören and Calisal (1998) dealt with the radiation problem; Kim and Yue (1987) computed the complete second-order radiation–diffraction problem, while Mavrakos (1988) found a numerical solution for the vertical drift force and pitch moment on axisymmetric floating bodies. Papanikolaou and Zaraphonitis (1987) worked on the second-order problem for shiplike bodies and, some years after, formalised the exact second-order theory and numerical solution for the wave–body interaction problem of arbitrarily shaped bodies (Zaraphonitis and Papanikolaou 1993), as well as Berkvens and Zandbergen (1998) and Ditzel et al. (1998).

8.2 Body-exact method

There exists two levels of complexity in the addiction of nonlinearities in the body-exact method. The first is by adding nonlinearities in the Froude–Krylov and hydrostatic forces, while the second involves the inclusion of the latter two forces and additional nonlinear radiation–diffraction forces.

8.2.1 Nonlinear Froude–Krylov/hydrostatic forces

The body-exact method extends linear potential flow models by adding nonlinearities in Froude–Krylov and hydrostatic forces, computing both on the exact instantaneous wetted surface $S_w(t)$ of the body

$$F_{\mathrm{NLFK}\,i}(t) = \iint_{S_w(t)} \frac{\partial \phi_0}{\partial t}(t) n_i \mathrm{d}s, \tag{205}$$

$$F_{Hi}(t) = -\iint_{S_w(t)} \rho g z(t) n_i \mathrm{d}s, \tag{206}$$

while radiation and diffraction forces remain linear and are computed using a fully linear code with linearized free-surface conditions at $z = 0$. The position of the body relative to the free-surface is updated at each time step to compute the new NLFK and hydrostatic forces.

Taking into account NLFK forces can significantly improve the results, without undue addition in computation time. The biggest challenge, in this method, is to calculate the exact surface between the body and the free surface, by modifying the mesh at each time step, or using a very refined mesh. To compute NLFK forces, a frequency-domain solution is usually no longer available and recourse is made to the time domain, as the body motion becomes non-sinusoidal. Taking into account FK nonlinearities allows nonlinear phenomena and instabilities to be demonstrated, such as parametric roll, that cannot be predicted using a fully linear code (see examples in Babarit et al. 2009; Giorgi and Ringwood 2018).

The body-exact code, developed by Gilloteaux (2010) at the LHEEA, uses a Green function approach. However, the code LAMP-2 (Treakle et al. 2000; Shin et al. 2003) supported by the US Navy, SWAN-2 (Grigoropoulos et al. 2011) developed by the group of Prof. Sclavounos at MIT, and WISH-2 (Kim et al. 2011) developed in Korea, use Rankine singularities. As Rankine singularities do not satisfy the radiation condition, a damping zone or a mixed-source formulation must be added to the domain to avoid reflection problems. Gilloteaux (2010) added second-order effects for linear radiation and diffraction forces, but it has been shown by Merigaud et al. (2012) that this leads to a significant increase in computation time for no commensurate improvement in accuracy.

8.2.2 Nonlinear radiation–diffraction

An improved version of the body-exact approach additionally takes into account nonlinearities in radiation and diffraction forces. In the literature, most of the potential flow codes are developed for ships and consider linear radiation and diffraction forces computed on the mean body position. However, when dealing with arbitrary shaped bodies, assumptions of linear forces may not be suitable. Some authors, like Bandyk (2009), Beck and Reed (2001), or Stern et al. (2014), briefly describe the complete (nonlinear hydrostatic, FK, diffraction and radiation force) body-exact nonlinear approach. Similar to the treatment of NLFK and hydrostatic forces, the radiation and diffraction forces are now computed on the exact instantaneous wetted surface, keeping the free-surface conditions linearized around $z = 0$. Some codes compute the nonlinear radiation–diffraction forces by linearising, around $z = 0$, the free-surface equations of the weak-scatterer approach (discussed in Sect. 8.3), such as LAMP-4 (Beck and Reed 2001), or the code WS_Cn, developed by the LHEEA in Nantes (Letournel 2015). Using the body-exact nonlinear radiation–diffraction option of WS_Cn is around three times faster than the weak-scatterer approach. In his thesis, Ferrant (1988) employs a body-exact nonlinear approach to compute the radiation problem only, using the Green function formulation.

In the case of the Green function formulation, the governing integral equations are given by

$$\begin{aligned} &2\pi\phi(M) + \iint_{S_w(t)} \left(\phi(P) \frac{\partial G^0}{\partial n}(M,P) \mathrm{d}S \right. \\ &\left. - \frac{\partial \phi(P)}{\partial n} G^0(M,P) \right) \mathrm{d}S \\ &= \int_0^t \mathrm{d}\tau \iint_{S_w(t)} \left(\phi(P) \frac{\partial G^f}{\partial n}(M,P) \mathrm{d}S \right. \\ &\left. - \frac{\partial \phi(P)}{\partial n} G^f(M,P) \right) \mathrm{d}S, \end{aligned} \tag{207}$$

where G^0 is the Rankine source term of the Green function, and G^f its time-dependent memory part, both defined in (132). After discretization in time, Eq. (207) becomes

$$\begin{aligned} &2\pi\phi(M)^{n+1} + \iint_{S_w^{n+1}} \left(\phi(P)^{n+1} \frac{\partial {G^0}^{n+1}}{\partial n}(M,P) \mathrm{d}S \right. \\ &\left. - \frac{\partial \phi}{\partial n}^{n+1}(P) {G^0}^{n+1}(M,P) \right) \mathrm{d}S \\ &= \int_0^{n+1} \mathrm{d}\tau \iint_{S_w(t)} \left(\phi(P) \frac{\partial G^f}{\partial n}(M,P) \mathrm{d}S \right. \\ &\left. - \frac{\partial \phi}{\partial n}(P) G^f(M,P) \right) \mathrm{d}S, \end{aligned} \tag{208}$$

at the $(n+1)$th time step. For the Rankine source formulation, the integral equation is

$$2\pi\phi(M)^{n+1} + \iint_{S_w \cup S_f^{n+1}} \phi(P)^{n+1} \frac{\partial G^R}{\partial n}(M, P)\mathrm{d}S - \iint_{S_w \cup S_f^{n+1}} \left(\frac{\partial \phi}{\partial n}\right)^{n+1} (P) G^R(M, P)\mathrm{d}S = 0. \quad (209)$$

The body-exact method, including nonlinear radiation–diffraction forces, needs significantly more computation time since the full Green function, or Rankine source, has to be re-computed at each time-step, due to changes in the relative positions of the body and the free-surface at each time step, considerably increasing the computation time.

Subramanian et al. (2018) proposed another kind of improved body-exact method, computing linear diffraction–radiation forces, but specifying the mean body position at each time step. Rajendran et al. (2016) uses Cummin's work in the time domain for radiation forces, a linear formulation derived following application of linear radiation boundary condition.

8.3 Weak-scatterer approach

The weak-scatterer approximation, originally introduced by Pawlowski (1994), is achieved by linearising the free-surface boundary condition around the instantaneous incident wave elevation, assuming that the perturbation potential is small compared to the incident one. The total velocity potential, and the free-surface elevation, can, therefore, be separated into incident and perturbation terms as

$$\begin{cases} \phi = \phi_0 + \phi_p, \\ \eta = \eta_0 + \eta_p. \end{cases} \quad (210)$$

The mixed Euler–Lagrange (MEL) approach, developed by Longuet-Higgins and Cokelet (1976), is employed to describe the nonlinear unsteady free-surface elevation, where Eulerian field equations are solved to obtain the fluid velocity, and the obtained velocity is used to track fluid particles on the free surface in a Lagrangian way. To simplify the MEL method, the free surface can be single-valued (as in Letournel et al. (2018)), assuming that the free-surface nodes can only move vertically $(x, y, z = \eta_0(x, y, t))$. Hence, overturning waves are not considered.

The mesh of the free surface is located at the position of the incident free-surface deformation. Thus, to update the perturbation component of the potential or elevation from the free-surface equations, it is necessary to follow the particles present on the incident free-surface. The differential operator, for a given particle, is given by

$$\frac{D_{0z}}{Dt} = \frac{\partial}{\partial t} + \frac{\partial \eta_0}{\partial t}\frac{\partial}{\partial z}. \quad (211)$$

The free-surface elevation $\eta(x, y, t)$ is independent of the z coordinate, which leads to

$$\frac{D_{0z}\eta}{Dt} = \frac{\partial \eta}{\partial t}. \quad (212)$$

The kinematic free-surface condition (3) can be rewritten as the decomposition of incident and perturbation terms as

$$\frac{\partial \eta_p}{\partial t} = -\frac{\partial \eta_0}{\partial t} + \frac{\partial}{\partial z}\left(\phi_0 + \phi_p\right) - \nabla\left(\phi_0 + \phi_p\right).\nabla\left(\eta_0 + \eta_p\right) \quad \text{on } z = \eta(x, y). \quad (213)$$

Equation (213) is expressed on the exact free-surface position $z = \eta(x, y)$. In the case of the weak-scatterer approach, the equation is moved on the incident free-surface elevation, by applying a Taylor expansion on the perturbation terms η_p, assumed small compared to the incident terms. Second-order perturbation terms, assumed negligible, are then removed. The kinematic free-surface condition becomes

$$\frac{\partial \eta_p}{\partial t} = -\frac{\partial \eta_0}{\partial t} + \frac{\partial}{\partial z}\left(\phi_0 + \phi_p\right) - \nabla\phi_0.\nabla\eta_0 - \nabla\phi_p.\nabla\eta_0 - \nabla\phi_0.\nabla\eta_p + \eta_p\left(\frac{\partial^2\phi_0}{\partial z^2} - \frac{\partial \nabla\phi_0}{\partial z}.\nabla\eta_0\right) \quad \text{on } z = \eta_0(x, y). \quad (214)$$

The dynamic free-surface boundary condition (3) can be expressed, using the differentiation operator (211), as

$$\frac{D_{0z}\phi}{Dt} = \frac{\partial \phi}{\partial t} + \frac{\partial \eta_0}{\partial t}\frac{\partial \phi}{\partial z} = -g\eta - \frac{1}{2}\nabla\phi.\nabla\phi + \frac{\partial \eta_0}{\partial t}\frac{\partial \phi}{\partial z} \quad \text{on } z = \eta(x, y). \quad (215)$$

Using the decomposition between incident and perturbation components, we obtain

$$\begin{aligned} \frac{D_{0z}\phi_p}{Dt} &= -\frac{D_{0z}\phi_0}{Dt} - g(\eta_0 + \eta_p) \\ &\quad -\frac{1}{2}\nabla\left(\phi_0 + \phi_p\right).\nabla\left(\phi_0 + \phi_p\right) \\ &\quad +\frac{\partial \eta_0}{\partial t}\frac{\partial}{\partial z}\left(\phi_0 + \phi_p\right) \\ &= -\frac{\partial \phi_0}{\partial t} - g(\eta_0 + \eta_p) \end{aligned}$$

$$-\frac{1}{2}\nabla\left(\phi_0+\phi_p\right).\nabla\left(\phi_0+\phi_p\right)$$
$$+\frac{\partial\eta_0}{\partial t}\frac{\partial\phi_p}{\partial z}\quad\text{on } z=\eta(x,y). \tag{216}$$

Similar to the kinematic free-surface condition (214), the dynamic free-surface condition is expressed on the incident free-surface elevation using a Taylor expansion of the perturbation term η_p, removing all the second-order perturbation terms as

$$\begin{aligned}\frac{D_{0z}\phi_p}{Dt} &= -\frac{\partial\phi_0}{\partial t}-g(\eta_0+\eta_p)\\ &\quad -\frac{1}{2}\nabla\phi_0.\nabla\phi_0-\nabla\phi_0.\nabla\phi_p+\frac{\partial\eta_0}{\partial t}\frac{\partial\phi_p}{\partial z}\\ &\quad -\eta_p\left(\frac{\partial^2\phi_0}{\partial z\partial t}+\frac{\partial\nabla\phi_0}{\partial z}.\nabla\phi_0\right)\quad\text{on } z=\eta_0(x,y).\end{aligned} \tag{217}$$

The body boundary condition is computed on the wetted surface of the body, by taking into account the instantaneous incident wave elevation. In Letournel et al. (2018), the problem is solved thanks to the implicit method (reviewed in Sect. 7.2.4).

The weak-scatterer assumption requires the problem to be solved with Rankine singularities since the free-surface equations are no longer linear. The codes SWAN-4 (Grigoropoulos et al. 2011), WISH-3 (Kim et al. 2011), and the code WS_Cn (Letournel et al. 2018) use a damping beach to remove the radiation condition problems of the the Rankine source, whereas LAMP-4 (Shin et al. 2003) uses the hybrid method. Letournel et al. (2014) compared the weak-scatterer approach with a fully nonlinear model for a heaving point absorber (HPA), and an oscillating wave surge converter (OWSC) in Letournel et al. (2018). Although it is not straightforward to compare two codes, Letournel et al. (2018) show good agreement between the two methods, the weak-scatterer approach being an order of magnitude faster than the fully nonlinear method, and CPU time being roughly two orders of magnitude greater than the real time simulated. However, the weak-scatterer code can still yield the response amplitude operator (RAO) for a set of 70 frequencies in a reasonable CPU time. The free-surface mesh size is around 10–20 times bigger than the characteristic length of the body, in the vicinity of the body. By simplifying the assumption of the free-surface boundary condition, and considering linearized free-surface elevation around the $z = 0$ plane, the problem becomes the body nonlinear approach developed in Sect. 8.2.2.

8.4 Fully nonlinear models

The development of fully nonlinear wave models, also called numerical wave tanks (NWTs), has mainly been developed for 2D problems in the 1990s, and in 3D since the 2000s. Since no assumptions are made on the body motion and wave steepness, large amplitude motion and extreme sea states can be considered. The development of fully nonlinear models has been possible thanks to the pioneering work of Longuet-Higgins and Cokelet (1976), who introduced the so-called mixed Eulerian–Lagrangian (MEL) method. The MEL method can compute fully nonlinear free-surface motion in time domain, by solving Eulerian field equations to obtain the fluid velocity, which then follows fluid particles on the free-surface in a Lagrangian way. Unlike the models presented previously (linear, body exact and weak scatterer in Sects. 4, 8.2 and 8.3, respectively), neither the incident free-surface elevation nor the incident potential are known, and form part of the unknowns of the problem. The incident wave is then produced by flap type or piston-like wavemakers, as for real wave tanks. The first 2D NWT dealing with a freely moving body was that of Vinje and Brevig (1981), who introduced the mode decomposition method. Koo and Kim (2004) analysed a freely floating-body simulation using a 2D fully nonlinear numerical wave tank, comparing fully nonlinear and body-exact nonlinear approaches. Their conclusion was that body nonlinearities are much more important than free-surface nonlinearities, when the body motion is near its resonance area. However, free-surface nonlinearities have a greater impact than body nonlinearities when drift forces are concerned. The so-called QALE-FEM method (once-off meshing) was detailed by Yan and Ma (2007), analysing the nonlinear interaction between steep waves and 2D floating bodies.

Ma et al. (2001) were the first to attempt 3D NWT simulations, using an iterative method. Relatively few developments have been undertaken in 3D for free motions of floating bodies, with some notable exception (e.g. Bai and Taylor 2009), and the 2D QALE-FEM in Yan and Ma (2007) was extended to 3D in Ma and Yan (2009).

9 Conclusions

Boundary element methods have become popular in a variety of application areas, providing a computationally attractive means of calculating hydrodynamic forces on floating, and fixed, objects. However, boundary element method comprise a large family of methods which are still under development. They can be classified into time domain and frequency domain, linear and several nonlinear variations progressively from weakly to fully nonlinear, and methods which can employ either (or both of) Green or Rankine sources. In addi-

tion, they can be applied to both objects which have non-zero or zero mean forward velocity, but not all methods or algorithms can be applied to both of these classes.

Consideration of the methods reviewed in terms of modeling fidelity and computational complexity leads us to the following reflections with respect to future methods that might emerge to satisfy the needs of wave energy:

Green function vs Rankine singularity: The Green function is attractive because it automatically satisfies both the free surface boundary condition and the far field radiation condition, therefore, avoiding meshing of the free surface and special treatment of radiated waves (e.g. hybrid method). However, this approach limits the method to linearised free surface conditions and introduces irregular frequencies that must then be removed. Hybrid methods can deal with the radiation condition effectively but at some computational cost.

Body exact methods: The review did not discover any method that combines body exact methods with close to the computational efficiency of linearised boundary element methods. Non-linear Froude–Krylov methods do not satisfy the Fidelity requirement introduced in Sect. 1.1 since some geometries (for example thin plates) are dominated by scattering and radiation forces with minimal Froude–Krylov forces. A body-exact method with the computational efficiency close to that of the linear methods is desirable as the minimally non-linear method that might satisfy all of the requirements introduced in Sect. 1.1.

Fully non-linear potential flow (NWT): NWT is unlikely to be a useful tool for large-scale calculations due to computational complexity and long run times. However, a general purpose implementation of a NWT might be useful for the validation of other methods and assessment of the impacts of assumptions made. A general purpose NWT would probably only be useful for as part of a hybrid method since far field radiation effects are important and pure NWT implementations are subject to reflections at the tank walls.

In wave energy application, the focus is on devices with mean zero forward velocity, both fixed and floating. A wide variety of commercial and non-commercial tools for boundary element hydrodynamic calculations exist and this review attempts to articulate the historical development of boundary element methods, as well as detailing the differences between various implementations, to facilitate judicious selection for future modelling of wave energy devices. This review is also indented to provide a useful platform for the further development of boundary element methods, particular with application to wave energy systems.

Acknowledgements This paper is based on upon work supported by Wave Venture and Enterprise Ireland under Innovation Voucher IV-2018-3114 and by Science Foundation Ireland under Grant No. 13/IA/1886. The authors are also grateful for useful discussions with Pierre Ferrant, Gérard Delhommeau, Aurélien Babarit, and Jean-Christophe Gilloteaux of Ecole Centrale Nantes.

References

Aubault A, Ertekin RC (2016) Stability of offshore systems. In: Xiros D (ed) Handbook of ocean engineering, chapter 34. Springer, pp 755–785

Babarit A, Delhommeau G (2015) Theoretical and numerical aspects of the open source BEM solver NEMOH. In: Proceedings of the 11th European wave and tidal energy conference, Nantes

Babarit A, Mouslim H, Clément A, Laporte-Weywada P (2009) On the numerical modelling of the non linear behaviour of a wave energy converter. In: ASME 2009 28th international conference on ocean, offshore and arctic engineering, Honolulu. American Society of Mechanical Engineers, pp 1045–1053

Bai KJ, Yeung RW (1974) Numerical solutions of free-surface flow problems. In: Proc. 10th symp. naval hydrodyn. office of naval research, Cambridge, pp 609–641

Bai W, Taylor RE (2009) Fully nonlinear simulation of wave interaction with fixed and floating flared structures. Ocean Eng 36(3–4):223–236

Baker GR, Meiron DI, Orszag SA (1989) Generalized vortex methods for free surface flow problems. II: radiating waves. J Sci Comput 4:237–259

Bandyk PJ (2009) A body-exact strip theory approach to ship motion computations. PhD thesis, University of Michigan

Beck RF, Reed A (2001) Modern seakeeping computations for ships. In: Twenty-third symposium on naval hydrodynamics, office of naval research, Bassin d'Essais des Carenes, National Research Council, Washington DC

Berhault C, Le Buhan P, Molin B, Bougis J (1992) Diodore: a numerical tool for frequency and time domain analysis of the behaviour of moored or towed floating structures. In: 4th intl conf on computer aided design manufacture and operation in the marine and offshore industries, Madrid, pp 721–740

Berkvens PJF, Zandbergen PJ (1998) Nonlinear unsteady 3-d motion of freely floating bodies. In: EUROMECH 374: recent computational developments in steady and unsteady naval hydrodynamics, Poitiers, pp 53–71

Bingham HB (2016) A note on the relative efficiency of methods for computing the transient free-surface Green function. Ocean Eng 120:15–20

Bochner S (1948) Vorlesungen über Fouriersche integrale. Chelsea Publishing Company, New York

Bratland A, Newman FKJ (1997) Time domain calculations in finite water depth. In: Proc. 12th int. workshop water waves float. bodies, Marseille, pp 13–17

Bull D, Roberts J, Malins R, Babarit A, Weber J, Dykes K, Costello R, Kennedy B, Neilson K, Bittencourt C (2016) Systems engineering applied to the development of a wave energy farm. In: Progress in renewable energies offshore: proceedings of the 2nd international conference on renewable energies, 2016 (RENEW2016). Taylor & Francis Books Ltd, pp 189–196

Cao Y, Beck RF, Schultz WW (1994) Nonlinear motions of floating bodies in incident waves. In: Proceedings of the 9th international workshop on water waves and floating bodies (IWWWFB), Kuju, pp 33–37

Chen XB (1993) Evaluation de la fonction de Green du problème de diffraction-radiation en profondeur d'eau finie - une nouvelle méthode rapide et précise. In: Actes des 4e Journées de l'Hydrodynamique, antes (France), Nantes, pp 371–384

Chen ZM (2018) New formulation of the finite depth free surface Green function. arXiv

Chuang J, Qiu W, Peng H (2007) On the evaluation of time-domain Green function. Ocean Eng 34:962–969

Clément A (1999b) Using differential properties of the Green function in seakeeping computational codes. In: 7th int. conf. numerical ship hydrodynamics, Nantes, France, pp 6.5 (1–15)
Clément A (2013) A second order ordinary differential equation for the frequency domain Green function. In: 28th international workshop on water waves and floating bodies, Marseille, p 4
Clément A (1999a) An ordinary differential equation for the Green function of time-domain free-surface hydrodynamics. J Eng Math 33(2):201–217
Cointe R (1989) Nonlinear simulation of transient free surface flows. In: 5th intl. conference numerical ship hydrodynamics, Hiroshima, pp 239–250
Cointe R (1991) Nonlinear and linear motion of a rectangular barge in a perfect fluid. In: Proceeding of the 18th symposium on naval hydrodynamics, Washington DC, pp 85–100
Costello R, Nielsen K, Weber J, Tom N, Roberts J (2019) Wavesparc: evaluation of innovation techniques for wave energy. In: Proceedings EWTEC 2019
Cummins WE (1962) The impulse response function and ship motions. In: Schiffstechnik, pp 101–109
Daubisse JC (1981) Some results on approximation by exponential series applied to hydrodynamics problems. In: Proc. 3rd intern. conf. numer. ship hydro., Paris
Davidson J, Costello R (2020) Efficient nonlinear hydrodynamic models for wave energy converter design—a scoping study. J Mar Sci Eng 8(1):35
Dawson CV (1977) A practical computer method for solving ship-wave problems. In: Proceedings of the second international conference on numerical ship hydrodynamics. University of California, Berkeley, pp 30–38
Delhommeau G (1989) Amélioration des performances des codes de calcul de diffraction-radiation au prenier ordre. In: 2 émes Journees de L'Hydrodynamique, Nantes, pp 69–88
Delhommeau G (1993) Seakeeping codes AQUADYN and AQUAPLUS. In: 19th WEGMENT school. Numerical simulation of hydrodynamics: ship and offshore structures, Nantes, pp 40–90
Ditzel A, Huijsmans RHM, Prins H (1998) Slowly varying wave drift forces in shallow water at forward speed. In: EUROMECH 374: recent computational developments in steady and unsteady naval hydrodynamics, Poitiers, pp 81–101
Dombre E, Benoit M, Violeau D, Peyrard C, Grilli ST (2015) Simulation of floating structure dynamics in waves by implicit coupling of a fully non-linear potential flow model and a rigid body motion approach. J Ocean Eng Mar Energy 1:55–76
Dommermuth DG, Yue DKP (1987) Numerical simulations of nonlinear axisymmetric flows with a free surface. J Fluid Mech 178:195–219
Drimer N, Agnon Y (1994) A hybrid boundary element method for second-order wave-body interaction. Appl Ocean Res 16(1):27–45
Erdélyi A (1956) Asymptotic expansions. Number 3. Courier Corporation. Dover Publications, Inc.
Ertekin RC, Rodenbusch G (2016) Wave, current and wind loads. In: Xiros D (ed) Handbook of ocean engineering, chapter 35. Springer, pp 787–818
Faltinsen OM (1975) Motions of large structures in waves at zero Froude number. Norske Veritas (90), 1975
Faltinsen OM (1977) Numerical solution of transient nonlinear free-surface motion outside or inside moving bodies. In: Proc. 2nd int. conf. on num. ship hydrodyn. University of California, Berkeley, pp 347–357
Faltinsen OM (1991) Sea loads on ships and offshore structures. Cambridge University Press, Cambridge
Ferrant P (1988) Radiation d'ondes de gravité par les déplacements de grande amplitude d'un corps immergé : comparaison des approches fréquencielle et instationnaire. PhD thesis, Ecole Centrale de Nantes
Finkelstein AB (1957) The initial value problem for transient water waves. Commun Pure Appl Math 10:511–522
Gilloteaux JC (2010) Mouvements de grande amplitude d'un corps flottant en fluide parfait. Application à la récupération de l'énergie des vagues. PhD thesis, Ecole Centrale de Nantes
Giorgi G, Ringwood JV (2018) Articulating parametric resonance for an owc spar buoy in regular and irregular waves. J Ocean Eng Mar Energy 4(4):311–322
Giorgi G, Retes M Penalba, Ringwood JV (2016) Nonlinear hydrodynamic models for heaving buoy wave energy converters. In: Asian wave and tidal energy conference, Singapore
Gören Ö, Calisal SM (1998) A hybrid method for second-order wave radiation by an oscillating axisymmetric cylinder. In: EUROMECH 374: recent computational developments in steady and unsteady naval hydrodynamics, Poitiers, pp 267–274
Grigoropoulos GJ, Katsikis C, Chalkias DS (2011) Experimental verification of the linear and non-linear versions of a panel code. Int J Nav Archit Ocean Eng 3:27–36
Guerber E (2011) Numerical modelling of nonlinear interactions of waves with submerged structures: applied to the simulation of wave energy converters. PhD thesis, Université Paris Est
Havelock T (1955) Waves due to a floating sphere making periodic heaving oscillations. Proc R Soc Lond Ser A Math Phys Sci 231:1–7
Huang Y (1997) Nonlinear ship motions by a Rankine panel method. PhD thesis, Massachusetts Institute of Technology
HydroStar Version 7-3 (2016) User manual
Israeli M, Orszag SA (1981) Approximation of radiation boundary conditions. J Comput Phys 41:115–135
John F (1950) On the motion of floating bodies II. Simple harmonic motions. Commun Pure Appl Math 3:45–101
Kashiwagi M (2000) Non-linear simulations of wave-induced motions of a floating body by means of the mixed Eulerian-Lagrangian method. Proc Inst Mech Eng Part C J Mech Eng Sci 214(6):841–855
Kellogg OD (1954) Foundations of Potential Theory. Dover Publications Inc, New York
Kim MH, Yue D (1987) Second order diffracted waves around an axisymmetric body. In: Proceedings of the 2nd international workshop on water waves and floating bodies, held University Bristol, UK, 16–19 March 1987
Kim Y (1999) Computation of higher-order hydrodynamic forces on ships and offshore structures in waves. PhD thesis, Massachusetts Institute of Technology
Kim Y (2003) Artificial damping in water wave problems II: application to wave absorption. Int J Offshore Polar Eng, 13(2)
Kim WD (1965) On the harmonic oscillations of a rigid body on a free surface. J Fluid Mech 21:427
Kim Y, Kring DC, Sclavounos PD (1997) Linear and nonlinear interactions of surface waves with bodies by a three-dimensional Rankine panel method. Appl Ocean Res 19:235–249
Kim Y, Kim KH, Kim JH, Kim T, Seo MG, Kim Y (2011) Time-domain analysis of nonlinear motion responses and structural loads on ships and offshore structures: development of WISH programs. Int J Nav Archit Ocean Eng 3:37–52
King B (1987) Time-domain analysis of wave exciting forces on ships and bodies. PhD thesis, University of Michigan
Koo W, Kim MH (2004) Freely floating-body simulation by a 2d fully nonlinear numerical wave tank. Ocean Eng 31(16):2011–2046
Kring DC (1994) Time domain ship motions by a three-dimensional Rankine panel method. PhD thesis, MIT
Lee CH, Newman JN (2005) Computation of wave effects using the panel method. In: WIT transactions on state-of-the-art in science

and engineering (in numerical models in fluid structure interaction, Ch.6), vol 18, WIT Press
Lee CH, Sclavounos PD (1989) Removing the irregular frequencies from integral equations in wave-body interactions. J Fluid Mech 207:393–418
Letournel L (2015) Développement d'un outil de simulation numérique basé sur l'approche "Weak-Scatterer" pour l'étude des systèmes houlomoteurs en grands mouvements. PhD thesis, Ecole Centrale de Nantes
Letournel L, Ducrozet G, Babarit A, Ferrant P (2017) Proof of the equivalence of Tanizawa–Berkvens's and Cointe–van Daalen's formulations for the time derivative of the velocity potential for non-linear potential flow solvers. Appl Ocean Res 63:184–199
Letournel L, Chauvigné C, Gelly B, Babarit A, Ducrozet G, Ferrant P (2018) Weakly nonlinear modeling of submerged wave energy converters. Appl Ocean Res 75:201–222
Letournel L, Ferrant P, Babarit A, Ducrozet G, Harris JC, Benoit M, Dombre E (2014) Comparison of fully nonlinear and weakly nonlinear potential flow solvers for the study of wave energy converters undergoing large amplitude motions. In: 33rd international conference on ocean, offshore and arctic engineering, San Francisco, USA. ASME
Li ZF, Ren HL, Tong XW, Li H (2015) A precise computation method of transient free surface Green function. Ocean Eng 105:318–326
Li Z, Ren H, Liu R, Li H (2017) Time domain Rankine-green panel method for offshore structures. J Ocean Univ China 16(1):65–73
Liapis SJ (1986) Time-domain analysis of ship motions. PhD thesis, University of Michigan
Lin WN, Newman JN, Yue DKP (1985) Nonlinear forced motions of floating bodies. In: Proceedings of 15th symposium on naval hydrodynamics, Washington DC, pp 33–48
Lin WN, Zhang S, Weems K, Yue DKP (1999) A mixed source formulation for nonlinear ship motion and wave load simulations. In: Proc. 7th international conference on numerical ship hydrodynamics, Nantes, pp 1–12
Linton CM, McIver P (2001) Handbook of mathematical techniques for wave-structure interactions. Chapman and Hall/CRC, Boca Raton
Liu Y, Falzarano JM (2017a) A method to remove irregular frequencies and log singularity evaluation in wave-body interaction problems. J Ocean Eng Mar Energy 3(2):161–189
Liu Y, Falzarano JM (2017b) Irregular frequency removal methods: theory and applications in hydrodynamics. Mar Syst Ocean Technol 12:49–64
Liu S, Papanikolaou AD (2011) Time-domain hybrid method for simulating large amplitude motions of ships advancing in waves. Int J Nav Archit Ocean Eng 3(1):72–79
Liu Y, Iwashita H, Hu C (2015) A calculation method for finite depth free-surface green function. Int J Nav Archit Ocean Eng 7:375–389
Longuet-Higgins MS, Cokelet ED (1976) The deformation of steep surface waves on water-I. A numerical method of computation. Proc R Soc Lond A Math Phys Sci 350(1660):1–26
Lunde JK (1951) On the linearized theory of wave resistance for displacement ships in steady and accelerated motion. In: Trans soc naval archit mar eng, vol 59. Washington DC, pp 25–76
Ma QW, Yan S (2009) Qale-fem for numerical modelling of non-linear interaction between 3d moored floating bodies and steep waves. Int J Numer Methods Eng 78(6):713–756
Ma QW, Wu GX, Eatock Taylor R (2001) Finite element simulation of fully non-linear interaction between vertical cylinders and steep waves. Part 1: methodology and numerical procedure. Int J Numer Methods Fluids 36(3):265–285
Mavrakos SA (1988) The vertical drift force and pitch moment on axisymmetric bodies in regular waves. Appl Ocean Res 10(4):207–218
Merigaud A, Gilloteaux JC, Ringwood JV (2012) A nonlinear extension for linear boundary element methods in wave energy device modelling. In: Volume 4: offshore geotechnics; Ronald W. Yeung honoring symposium on offshore and ship hydrodynamics, Rio de Janeiro. ASME, p 615
Molin B (1979) Second-order diffraction loads upon three-dimensional bodies. Appl Ocean Res 1(4):197–202
Nakos DE, Sclavounos PD (1990) On steady and unsteady ship wave patterns. J Fluid Mech 215:263
Newman JN (1985) Algorithms for the free-surface Green function. J Eng Math 19:57–67
Newman JN (1992) The approximation of free-surface Green functions. Wave asymptotics, vol 107. Cambridge University Press, Cambridge, pp 108–135
Newman JN (2018) Marine hydrodynamics. The MIT Press, Cambridge
Noblesse F (1982) The Green function in the theory of radiation and diffraction of regular water waves by a body. J Eng Math 16(2):137–169
Ogilvie TF (1966) Recent progress toward the understanding and prediction of ship motions. In: Ship motions and drag reduction, pp 3–80
Ogilvie TF (1983) Second-order hydrodynamic effects on ocean platforms. In: Proceedings of the international workshop on ship and platform motions, Berkeley, pp 205–265
Ohmatsu S (1975) On the irregular frequencies in the theory of oscillating bodies in a free surface. In: Paper 48 of the Ship Research Institute, Ship Dynamics Division, Tokyo
Papanikolaou AD, Schellin TE (1992) A three-dimensional panel method for motions and loads of ships with forward speed. Ship Technol Res 39(4):145–154
Papanikolaou A (1985) On integral-equation-methods for the evaluation of motions and loads of arbitrary bodies in waves. Ingenieur-Archiv 55(1):17–29
Papanikolaou A, Zaraphonitis G (1987) On a improved method for the evaluation of second-order motions and loads on 3d floating bodies in waves. J Schiffstechnik Ship Technol Res 34:170–211
Pawlowski J (1994) A nonlinear theory of ship motion in waves. In: 19th symposium on naval hydrodynamics, Washington DC, pp 33–58
Penalba M, Giorgi G, Ringwood JV (2017) Mathematical modelling of wave energy converters: a review of nonlinear approaches. Renew Sustain Energy Rev 78:1188–1207
Peter MA, Meylan MH (2004) The eigenfunction expansion of the infinite depth free surface Green function in three dimensions. Wave Motion 40:1–11
Pidcock MK (1985) The calculation of Green's functions in three dimensional hydrodynamic gravity wave problems. Int J Numer Methods Fluids 5:891–909
Pinkster JA, Van Oortmerssen G (1978) Computation of the first and second order wave forces on oscillating bodies in regular waves. In: Proceedings of the 2nd international conference on numerical ship hydrodynamics, Berkeley
Rajendran S, Fonseca N, Guedes Soares C (2016) Prediction of vertical responses of a container ship in abnormal waves. Ocean Eng 119:165–180
Raven HC (1988) Variations on a theme by Dawson. In: 17th symposium on naval hydrodynamics, Washington, DC, pp 151–172
Roberts JD, Weber J, Laird D, Costello RP, Bull DL, Babarit A, Nielsen K, Bittencourt C, Kennedy B (2017) Cost time and risk assessment of different wec technology development paths. Technical report, Sandia National Lab (SNL-NM), Albuquerque
Sarpkaya T (1986) Force on a circular cylinder in viscous oscillatory flow at low Keulegan-Carpenter numbers. J Fluid Mech 165:61–71
Sclavounos PD (1996) Computation of wave ship interactions. Advances in Marine Hydrodynamics, Computational Mechanics Publications
Sclavounos PD, Nakos DE (1988) Stability analysis of panel methods for free-surface flows with forward speed. In: 17th symposium on naval hydrodynamics, Washington DC, pp 173–193

Scragg C, Talcott J (1991) Numerical solution of the "Dawson" free-surface problem using Havelock singularities. In: 18th symposium on naval hydrodynamics, Washington DC, pp 259–272

Sen D (1993) Numerical simulation of motions of two-dimensional floating bodies. J Ship Res 37(04):307–330

Shao YL (2010) Numerical potential-flow studies on weakly-nonlinear wave-body interactions with/without small forward speeds. PhD thesis, NTNU

Shin YS, Belenky VL, Lin WM, Weems KM, Engle AH, McTaggart K, Falzarano JM, Hutchinson BL, Gerigk M, Grochowalski S (2003) Nonlinear time domain simulation technology for seakeeping and wave-load analysis for modern ship design. Authors' closure. Trans Soc Nav Archit Mar Eng 111:557–583

Stern F, Sadat-Hosseini H, Mousaviraad M, Bhushan S (2014) Evaluation of seakeeping predictions. In: Larsson L, Stern F, Visonneau M (eds) Numerical ship hydrodynamics. Springer, Dordrecht, pp 141–202

Stoker JJ (1957) Water waves: the mathematical theory with applications, vol 4. Wiley, New York

Subramanian R, Rakesh NV, Beck RF (2018) An improved body-exact method to predict large amplitude ship roll responses. In: Volume 9: offshore geotechnics; honoring symposium for Professor Bernard Molin on marine and offshore hydrodynamics, Madrid. ASME

Tanizawa K (1995) A nonlinear simulation method of 3-D body motions in waves. J Soc Nav Archit Japan 178:179–191

Tanizawa K, Minami M (2001) Development of a 3d-NWT for simulation of running ship motions in waves. In: International workshop on water waves and floating bodies, Hiroshima, p 4

Telste J, Noblesse F (1986) Numerical evaluation of the Green function of water-wave radiation and diffraction. J Ship Res 30(02):69–84

Treakle TW, Mook DT, Liapis SJ, Nayfeh AH (2000) A time-domain method to evaluate the use of moving weights to reduce the roll motion of a ship. Ocean Eng 27:1321–1343

van Daalen EFG (1993) Numerical and theoretical studies of water waves and floating bodies. PhD thesis, University of Twente

Vinje T, Brevig P (1981) Nonlinear ship motions. In: Proc. 3rd int. conf. on num. ship hydro., Paris, pp 257–268

WADAM (2013) Frequency domain hydrodynamic analysis of stationary vessels. https://www.dnvgl.com/services/frequency-domain-hydrodynamic-analysis-of-stationary-vessels-wadam-2412. Accessed 02 Apr 2020

WAMIT Version 7-0 (2013) User manual. http://www.wamit.com. Accessed 02 Apr 2020

Wang CZ, Wu GX, Drake KR (2007) Interactions between nonlinear water waves and non-wall-sided 3d structures. Ocean Eng 34(8–9):1182–1196

Watson GN (1924) A treatise on the theory of Bessel functions. Bull Am Math Soc 30:362–364

Weber J (2012) Wec technology readiness and performance matrix–finding the best research technology development trajectory. In: Int. conf. on ocean energy (ICOE), Dublin

Weber JW, Laird D (2018) Structured innovation of high-performance wave energy converter technology. Technical report, National Renewable Energy Lab (NREL), Golden, CO

Weber J, Costello R, Ringwood J (2013) Wec technology performance levels (tpls)-metric for successful development of economic wec technology. In: Proceedings EWTEC 2013

Wehausen JV, Laitone EV (1960) Surface waves. In: Truesdell C (ed) Fluid dynamics/Strömungsmechanik. Encyclopedia of Physics/Handbuch der Physik. Springer, Berlin

Wenvang D, Yishan D (1999) Time-domain calculation of hydrodynamic forces on ships with large flare (part 2: three-dimensional case). Int Ship Prog 46:223–232

Windt C, Davidson J, Ringwood JV (2018) High-fidelity numerical modelling of ocean wave energy systems: a review of computational fluid dynamics-based numerical wave tanks. Renew Sustain Energy Rev 93:610–630

Wu GX, Taylor R Eatock (1996) Transient motion of a floating body in steep water waves. In: Proc. 11th workshop on water waves and floating bodies, Hamburg

Wu H, Zhang C, Zhu Y, Li W, Wan D, Noblesse F (2017) A global approximation to the Green function for diffraction radiation of water waves. Eur J Mech Fluids 65:54–64

Wu H, Liang H, Noblesse F (2018) Wave component in the Green function for diffraction radiation of regular water waves. Appl Ocean Res 81:72–75

Wynn P (1956) On a device for computing the $e_m(s_n)$ transformation. In: Mathematical tables and other aids to computation, pp 91–96

Xie C (2019) An efficient method for the calculation of the free-surface Green function using ordinary differential equations. PhD thesis, Ecole Centrale de Nantes

Xie C, Choi Y, Rongère F, Clément A, Delhommeau G, Babarit A (2018a) Comparison of existing methods for the calculation of the infinite water depth free-surface Green function for the wave-structure interaction problem. Appl Ocean Res 81:150–163

Xie C, Babarit A, Rongère F, Clément A (2018b) Use of Clement's ODEs for the speedup of computation of the Green function and its derivatives for floating or submerged bodies in deep water. In: 37th international conference on ocean, offshore and arctic engineering, Madrid. ASME

Yan S, Ma QW (2007) Numerical simulation of fully nonlinear interaction between steep waves and 2d floating bodies using the qale-fem method. J Comput Phys 221(2):666–692

Yeung RW (1982) Numerical methods in free-surface flows. Annu Rev Fluid Mech 14:395–442

Zaraphonitis GN, Papanikolaou AD (1993) Second-order theory and calculations of motions and loads of arbitrarily shaped 3d bodies in waves. Mar Struct 6(2–3):165–185

Zhu X (1994) Irregular frequency removal from the boundary integral equation for the wave-body problem. PhD thesis, Massachusetts Institute of Technology